Journal of
Composites Science

MDPI

Review

Progress in Thin-Film Photovoltaics: A Review of Key Strategies to Enhance the Efficiency of CIGS, CdTe, and CZTSSe Solar Cells

Sivabalan Maniam Sivasankar *, Carlos de Oliveira Amorim * and António F. da Cunha

Department of Physics, i3N, University of Aveiro, 3810-193 Aveiro, Portugal; antonio.cunha@ua.pt
* Correspondence: sivabalanms@ua.pt (S.M.S.); amorim5@ua.pt (C.d.O.A.)

Abstract: Thin-film solar cells (TFSCs) represent a promising frontier in renewable energy technologies due to their potential for cost reduction, material efficiency, and adaptability. This literature review examines the key materials and advancements that make up TFSC technologies, with a focus on Cu(In,Ga)Se_2 (CIGS), cadmium telluride (CdTe), and Cu_2ZnSnS_4 (CZTS) and its sulfo-selenide counterpart $Cu_2ZnSn(S,Se)_4$ (CZTSSe). Each material's unique properties—including tuneable bandgaps, high absorption coefficients, and low-cost scalability—make them viable candidates for a wide range of applications, from building-integrated photovoltaics (BIPV) to portable energy solutions. This review explores recent progress in the enhancement of power conversion efficiency (PCE), particularly through bandgap engineering, alkali metal doping, and interface optimization. Key innovations such as silver (Ag) alloying in CIGS, selenium (Se) alloying in CdTe, and sulfur (S) to Se ratio optimization in CZTSSe have driven PCE improvements and expanded the range of practical uses. Additionally, the adaptability of TFSCs for roll-to-roll manufacturing on flexible substrates has further cemented their role in advancing renewable energy adoption. Challenges remain, including environmental concerns, but ongoing research addresses these limitations, paving the way for TFSCs to become a crucial technology for transitioning to sustainable energy systems.

Keywords: thin-film solar cells; photovoltaics; CIGS; CdTe; CZTS; bandgap engineering

Academic Editor: Joshua M. Pearce

Received: 16 January 2025
Revised: 26 February 2025
Accepted: 17 March 2025
Published: 20 March 2025

Citation: Sivasankar, S.M.; Amorim, C.d.O.; Cunha, A.F.d. Progress in Thin-Film Photovoltaics: A Review of Key Strategies to Enhance the Efficiency of CIGS, CdTe, and CZTSSe Solar Cells. *J. Compos. Sci.* **2025**, *9*, 143. https://doi.org/10.3390/jcs9030143

1. Introduction

TFSCs have attracted significant interest due to their potential to lower costs, increase flexibility, and scale up production for a wide range of solar applications. By using far less material than traditional silicon-based cells, TFSCs reduce both material and production costs, making them an attractive choice for sustainable energy solutions.

TFSCs use absorber layers only a few micrometres thick, unlike conventional crystalline silicon cells that require thick (>100 µm), high-purity wafers. This efficient use of materials, along with versatile deposition methods like sputtering, thermal evaporation, and solution processing, significantly cuts down production costs [1–3]. The use of earth-abundant and non-toxic materials in some TFSC technologies further enhances their sustainability by minimizing their environmental footprint [4–6].

Another major advantage of TFSCs is their potential for roll-to-roll manufacturing, which allows continuous deposition on flexible substrates and enables the large-scale production of lightweight, flexible solar modules [7–9]. These modules can be integrated into various surfaces such as rooftops, facades, and vehicles [3,10,11]. Roll-to-roll processing reduces production time and labour, supporting the development of lightweight, bendable

solar panels that are ideal for portable and wearable technologies [9,12]. TFSCs are particularly well-suited for BIPV, where solar panels are embedded directly into multifunctional construction elements, allowing buildings to generate their own energy [13,14]. This integration is especially advantageous in urban environments with limited space, promoting energy self-sufficiency and sustainability.

The lightweight and flexible characteristics of TFSCs make them suitable for mobile applications, such as solar-powered vehicles, portable chargers, and aerospace technologies [7,8,13]. These features are particularly valuable in remote or underdeveloped regions, where conventional energy infrastructure may be lacking. TFSCs can provide reliable power sources for communication devices, lighting, and essential equipment in off-grid areas, significantly improving quality of life. They are also valuable in emergency scenarios, such as natural disasters, where the rapid deployment of power sources is critical [7,8,13]. Additionally, their scalability and adaptable deposition techniques, like sputtering, chemical vapour deposition (CVD), and solution processing, make TFSCs suitable for mass production and utility-scale installations [9,12]. Their lower temperature requirements reduce energy consumption, supporting the use of diverse substrates, including heat-sensitive materials, and contributing to the transition to cleaner energy on a larger scale [15–19]. Furthermore, TFSCs drive innovation in solar technology design, enabling integration into challenging environments such as electric vehicles and aerospace technologies. For example, TFSCs can extend the driving range of electric vehicles by providing supplementary power or reduce the weight of satellites and other high-altitude technologies, where PCE is critical.

TFSCs represent a major advancement in solar technology, offering a combination of low cost, flexibility, and scalability. These qualities position them as key players in the future of renewable energy, suitable for diverse applications ranging from building materials to portable devices. As research continues to improve their PCE and lower costs, TFSCs are expected to play an increasingly vital role in achieving global renewable energy goals and reducing dependence on fossil fuels. By integrating TFSCs into everyday infrastructure, solar energy can become more accessible and widespread.

In recent years, solar cells based on perovskite materials have emerged as a disruptive photovoltaic technology, garnering significant research interest due to their impressive efficiency gains and low-temperature processing capabilities. However, despite their potential, perovskite solar cells face considerable challenges related to long-term stability, environmental concerns linked to lead content, and obstacles in large-scale manufacturing.

Similarly, antimony-based materials like $Sb_2S_3Se_{3-x}$ and Sb_2Se_3 have emerged as promising candidates for thin-film photovoltaics due to their earth-abundant composition and favourable optoelectronic properties. Nonetheless, their current power conversion efficiencies are modest compared to established technologies, and issues related to material stability and interface engineering persist.

Other materials under investigation include bismuth-based compounds [5], tin-based perovskites [20], and various organic photovoltaics. While these materials offer potential advantages such as reduced toxicity and flexibility, they also face significant hurdles in terms of efficiency, stability, and large-scale manufacturability. In contrast, TFSCs made from CIGS, CdTe, and CZTSSe have already established themselves as viable alternatives to conventional silicon photovoltaics, supported by decades of research that underline their commercial deployment and ongoing advancements.

Given the fundamental differences in material properties, device physics, and technological maturity, this review will focus solely on these established thin-film technologies. We aim to examine the latest strategies for enhancing their efficiency and stability, providing a detailed perspective on the progress and future prospects of these commercially relevant

photovoltaics. Our analysis will intentionally exclude perovskite-based solutions, as they represent an entirely different research trajectory.

The rapid advancement of TFSCs has positioned them as a pivotal technology in the transition toward sustainable energy. However, the challenge of improving their PCE while keeping costs competitive remains significant. This review offers a comprehensive analysis of recent advancements in CIGS, CdTe, and CZTSSe, with an emphasis on successful strategies for performance enhancement. By consolidating recent research findings, we seek to guide future investigations into optimizing bandgap engineering, doping methods, and interface modifications to elevate TFSC efficiency further. Understanding these advancements is essential for researchers and industry stakeholders looking to accelerate the commercialization and large-scale deployment of TFSC technologies. The following sections will explore recent developments, ongoing research, and emerging applications that are propelling TFSC technology forward and defining its role in the renewable energy landscape.

2. Key Thin-Film Absorber Materials

2.1. CIGS

CIGS is a quaternary semiconductor material widely used in TFSCs. It has gained significant attention due to its excellent light-absorbing properties, which contribute to its high PCE. The general formula for CIGS is $Cu(In_{1-x}Ga_x)Se_2$, where "x" represents the gallium (Ga) content. In laboratory conditions, CIGS have achieved a PCE of over 23% [21], making it one of the highest-performing TFSC technologies [22]. Table 1 lists the progress of CIGS solar cell PCE over the years. Figure 1 highlights key advancements, such as CdS chemical bath deposition (CBD), Ga and sodium (Na) doping, and post-deposition treatments (PDT) with alkali metals, which have been instrumental in achieving these high PCE results. Recent research has also shown that alloying Ag into CIGS can increase the PCE to as high as 23.6%, positioning CIGS as a leading candidate in TFSCs [23]. Table 2 lists some of the commercial products available in the market utilizing this technology.

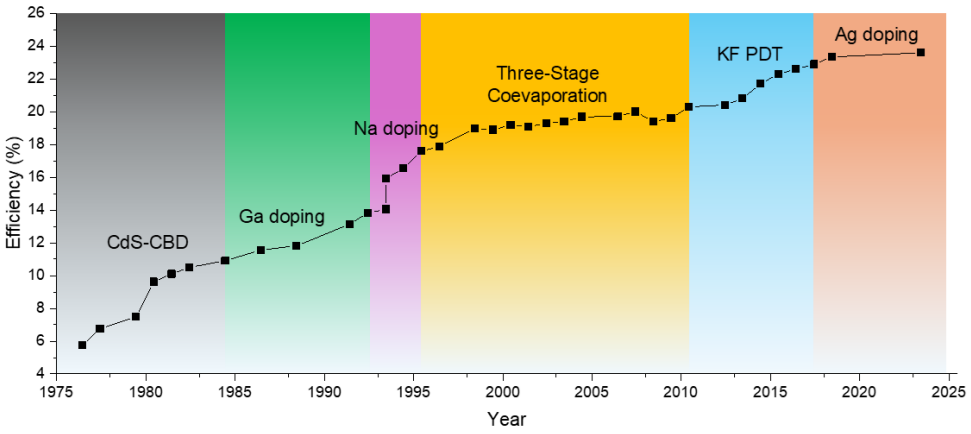

Figure 1. Efficiency evolution of CIGS solar cells, highlighting key strategies: CdS-CBD, Ga and Na doping, three-stage co-evaporation, KF PDT and Ag doping/alloying (data from research-cell efficiency, NREL).

One of the primary advantages of CIGS lies in its tuneable bandgap, which can be adjusted between approximately 1.0 eV and 1.7 eV by varying the ratio of indium (In) to Ga within the alloy [14,24,25]. Increasing the Ga content widens the bandgap, shifting the material's absorption spectrum from the infrared towards the visible region. This tunability provides CIGS with a competitive edge in photovoltaic (PV) applications, as it allows for the optimization of the material for specific requirements, including applications in

tandem or multijunction solar cells, where materials with different bandgaps are stacked to improve the overall PCE. The incorporation of Ga not only modifies the bandgap but also enhances the open circuit voltage (V_{oc}), which is crucial for improving the overall PCE of the solar cells.

Table 1. Evolution of efficiency in CIGS solar cells using different grading strategies and deposition techniques.

Year	CIGS Grading Strategy	V_{oc} (V)	J_{sc} (mA/cm^2)	FF (%)	η (%)	Ref.
1993	Physical vapour deposition (PVD)	0.7	–	–	12.2	[26]
1994	Co-evaporation of In, Ga, and Se	0.649	31.88	76.6	15.9	[27]
1996	PVD	0.642	31.9	73.7	15.1	[28]
2001	Three-stage process	0.691	33	76	16.7	[29]
2003	Co-evaporation	0.625	29.4	72	14.2	[30]
2003	Co-evaporation	0.66	31.9	76	16.1	[31]
2003	Three-stage process	0.689	35.71	78.12	19.2	[32]
2008	Co-evaporation	0.69	35.5	81.2	19.9	[33]
2011	Co-evaporation	0.74	35.4	77.5	20.3	[34]
2011	Three-stage process	0.665	31.1	73.6	15.5	[35]
2013	Co-evaporation	0.723	33.76	76.09	18.56	[36]
2015	Sequential evaporation	0.674/0.725	33.2/34.20	74.8/80.50	16.7/20.0	[37]
2016	Three-stage process	0.6	28	74	12.1	[38]
2017	Co-evaporation	0.718	35.9	76.8	19.9	[39]
2019	Three-stage process	0.498	37	74	13.6	[40]
2019	Three-stage process	0.61	30.53	60.71	11.7	[41]
2019	Co-evaporation	0.731	36.6	75.9	20.3	[42]
2019	Co-evaporation	0.65	28	70	12	[43]
2019	Sequential sputtering with sulfurization after selenization	0.73	41.9	79	23.35	[44]
2024	Co-evaporation	0.767	38.3	80.5	23.6	[23]

Table 2. Commercial manufacturers for CIGS solar modules and their module characteristics.

Manufacturer	Process	V_{oc} (V) *	J_{sc} (A) *	FF (%) *	η (%) *	Country	Ref
Solar Frontier	Sputtering	112	2.2	68.9	13.8	Japan	[45]
MiaSolé	Sputtering	37.8	4.58	70.7	17	USA	[46]
Ascent Solar	Co-evaporation	23	3.55	58	17.55	USA	[47]
Sunflare	Co-evaporation	36.6	7.5	67	15	USA	[48]
Eterbright Solar Corp.	Co-evaporation	74.2	2.32	69.6	14.9	Taiwan	[49]
DS New Energy	Sputtering	40.92	4.52	76.1	18.3	China	[50]
AVANCIS	Sputtering	24	10.5	79.3	17.7	Germany	[51]

* Values mentioned are module parameters.

A typical CIGS solar cell consists of a multilayer structure optimized to achieve high PCE (Figure 2). Cell preparation starts with a substrate, typically soda lime glass (SLG), but flexible polymers or metal foils can also be used depending on the intended application. On top of the substrate, a molybdenum (Mo) back contact layer is deposited, which serves as the electrical contact and provides good adhesion to the CIGS absorber layer. The CIGS layer is a p-type semiconductor material responsible for absorbing incident light and generating electron–hole pairs, which drive the PV process. On top of the absorber, a cadmium sulfide (CdS) buffer layer is deposited to form a p-n junction and promote charge carrier separation. A transparent window layer consisting of a transparent conducting oxide (TCO) layer such as zinc oxide (ZnO), is then applied to allow sunlight to pass through while facilitating charge carrier collection. An anti-reflective coating can be added

on top to minimize light loss. Each of these layers plays a crucial role in maximizing the performance of the solar cell by enhancing light absorption, charge carrier mobility, and overall PCE.

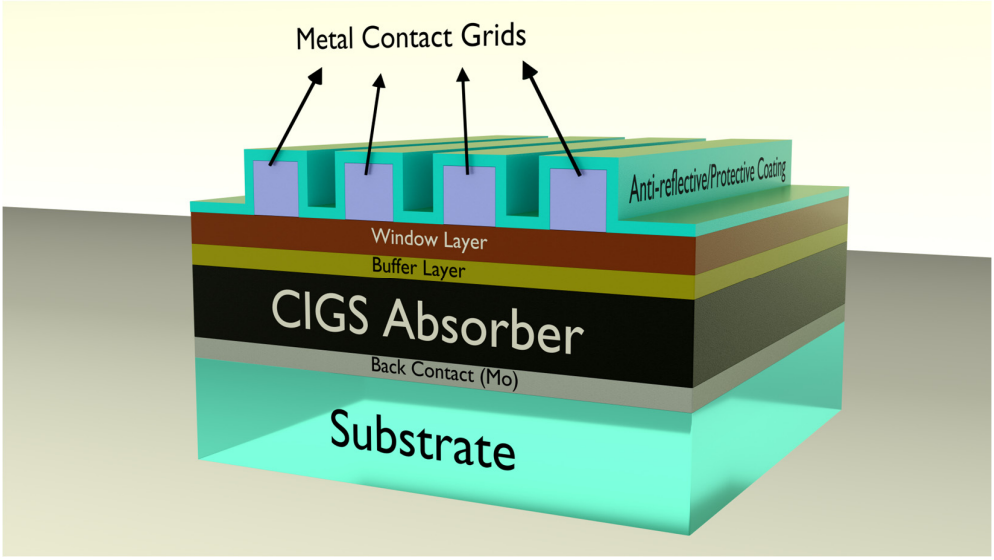

Figure 2. Illustration of the structure of a CIGS solar cell, depicting its key structural layers: the glass substrate, molybdenum back contact, CIGS absorber layer, buffer layer, window layer, a metal grid, and an anti-reflective and/or protective coating.

CIGS exhibits a high optical absorption coefficient, which allows for the use of thin absorber layers, typically around 2 µm thick [22,25]. The thin nature of these absorber layers reduces the amount of required raw material, leading to lower manufacturing costs while still retaining high performance. Moreover, the feasibility of utilizing flexible substrates makes CIGS solar cells highly suitable for lightweight and portable applications.

This combination of tuneable properties, high absorption coefficient, flexibility, and adaptability to different substrates makes CIGS one of the most promising materials for advancing TFSC technologies. However, their industrial scalability is hindered by the reliance on scarce and costly elements such as indium and gallium, which are also in demand by other industries. The deposition processes required to achieve high-performance CIGS films, such as co-evaporation and three-stage processes, involve precise control over precursor ratios and reaction conditions, making large-scale manufacturing more complex compared to other thin-film technologies. Moreover, the efficiency improvements in CIGS cells heavily depend on post-deposition alkali metal treatments, particularly with elements such as sodium, potassium, rubidium, and caesium.

While these treatments enhance carrier collection and passivation, they introduce additional fabrication steps that must be optimized for industrial-scale production. Another consideration for commercial implementation is the long-term stability of flexible CIGS modules. Although flexible and lightweight CIGS panels offer significant advantages for specific applications, concerns remain regarding the durability of encapsulation materials and mechanical stability under real-world conditions. Additionally, environmental and regulatory challenges arise due to the use of selenium and heavy metal alkali doping, necessitating appropriate waste management and recycling strategies.

2.2. CdTe

CdTe solar cells have emerged as a leading technology in the PV industry due to their cost-effectiveness, high PCE, and excellent stability. With a direct bandgap of approximately 1.45 eV, CdTe is particularly well-suited for solar energy conversion, as this value closely

aligns with the ideal range for absorbing sunlight and converting it into electricity [52–54]. This combination of a suitable bandgap and stability has made CdTe one of the most prominent thin-film technologies, significantly contributing to the global PV market [55].

The development of CdTe solar cells has been driven by continuous research and innovation, with a particular focus on optimizing fabrication techniques and understanding the fundamental properties of CdTe [52,56]. Researchers have explored various deposition methods, such as close-spaced sublimation (CSS) and CBD, to produce high-quality CdTe thin films with controlled properties [53,54,56]. These methods are crucial for determining the overall performance of CdTe solar cells.

A critical design feature of CdTe solar cells is the heterojunction (HJT) formed between CdTe and CdS [52,53,56]. The typical structure of CdTe solar cells employs a superstrate configuration, unlike the substrate configuration used in CIGS solar cells. As shown in Figure 3, the CdTe solar cell consists of several layers: the superstrate, a TCO layer, the CdS buffer layer, the CdTe absorber layer, and the back contact. Each of these layers plays a key role in determining the PCE and stability of the solar cell. This HJT is essential for facilitating charge separation and transport, which directly enhances the PCE of the solar cell [22,52,56]. Moreover, understanding the interdiffusion between the CdS and CdTe layers has proven to be vital for optimizing the device performance [52,56].

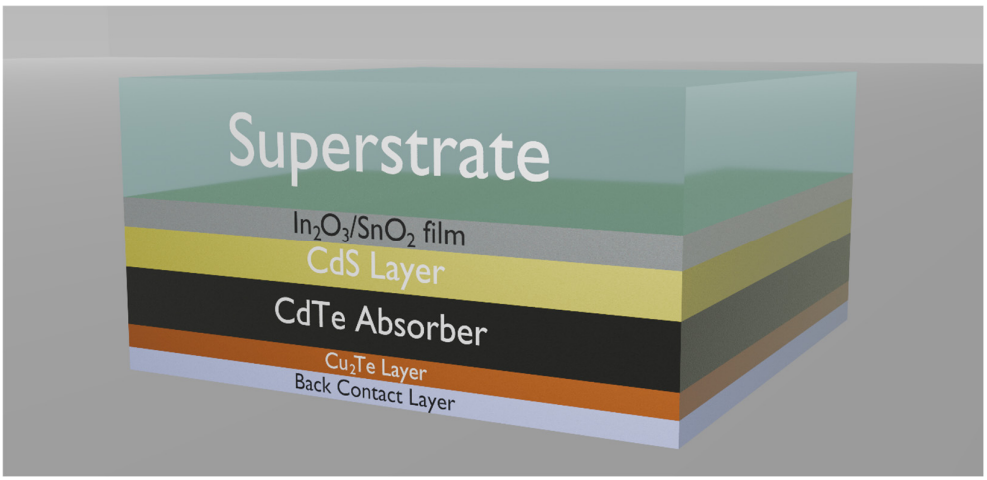

Figure 3. Illustration of the structure of a CdTe solar cell, depicting its key structural layers: the glass superstrate, TCO, CdS buffer layer, CdTe absorber layer, and back contact layer.

Bandgap engineering has also emerged as a key strategy for further improving the PCE of CdTe solar cells [22,52]. This approach involves precisely tuning the bandgap of the CdTe material to maximize sunlight absorption and improve charge carrier collection. By tailoring the bandgap, researchers can push the limits of CdTe solar cell PCE towards higher values [52,54].

Recent advancements in CdTe technology have led to remarkable efficiency gains, with lab-scale devices achieving over 23% PCE [21,52,56]. Key advancements are listed in Table 3 and further illustrated in Figure 4, highlight the evolution of doping, bandgap engineering, and back contact optimization, all driven by ongoing research and innovations in material quality. Companies like First Solar and other as listed in Table 4 have been instrumental in commercializing CdTe solar cells, capturing a significant share of the thin-film solar cell market [22,52]. To date, over 25 GW of CdTe-based power-generation modules have been installed globally, highlighting the growing adoption and success of this technology [52].

Table 3. Key CdTe world record cells, their cell parameters, and deposition methods.

Year	Deposition Method	V_{oc} (V)	J_{sc} (mA/cm^2)	FF (%)	η (%)	Ref
1992	Close-Spaced Sublimation (CSS)	0.843	25.1	74.5	15.8	[57]
2002	Electrodeposition	0.823	3.10	63	10.6	[58]
2012	Close-Spaced Sublimation (CSS)	–	–	–	14.4	[59]
2014	Vapour Transport Deposition (VTD)	0.87	30.25	79.4	21.0	[21]
2016	Vapour Transport Deposition (VTD)	0.89	31.40	79.3	22.4	[21]

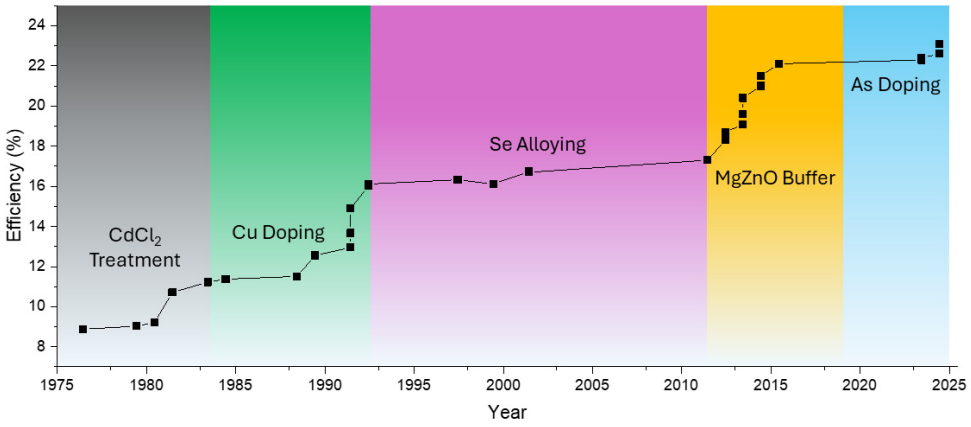

Figure 4. CdTe solar cell PCE evolution (1980–2024), highlighting key advancements: $CdCl_2$ treatment, Cu/As doping, CdSeTe alloying, MgZnO buffers, and grain boundary passivation (data from research-cell efficiency, NREL).

Table 4. Commercial manufacturers of CdTe solar modules and their module characteristics.

Manufacturer	Process	V_{oc} (V) *	J_{sc} (A) *	FF (%) *	η (%) *	Country	Ref
First Solar	Vapour Transport Deposition	228.8	3.08	78	19.7	USA	[60]
Solar Motion Electronics Co., Ltd.	-	123.5	1.25	71.4	-	Hong Kong	[61]
CSG PV Tech	-	123.5	3.66	66	13.89	China	[62]
Advanced Solar Power	-	119.5	1.36	64.6	14.58	China	[63]
CTF Solar	-	63.6	2.06	64.9	-	Germany	[64]

* Values mentioned are module parameters.

CdTe solar cells represent the most commercially successful thin-film photovoltaic technology, with gigawatt-scale production already established. However, CdTe manufacturing still faces challenges that affect its long-term viability. One of the primary concerns is the availability of tellurium (Te), a rare element predominantly obtained as a byproduct of copper refining. Fluctuations in Te supply and cost may impose constraints on future scalability. Additionally, the presence of cadmium (Cd) raises environmental and health concerns, requiring stringent regulations for handling and module disposal. While extensive recycling programmes have been developed to mitigate these risks [65,66], maintaining sustainable production remains a critical challenge. Despite its successes, CdTe solar cell technology faces ongoing scrutiny regarding the toxicity of Cd, making environmental considerations a key aspect of its industrial implementation. Addressing these concerns while continuing to enhance device performance remains a major focus of ongoing research [52,55].

Another key issue in CdTe solar cell performance is the development of stable, low-resistance back contacts. Copper-containing back contacts have been used to improve efficiency, but they can lead to device degradation over time due to copper diffusion [56,65,67]. Further advancements in back-contact engineering and passivation strategies are necessary to enhance long-term stability. In terms of large-scale manufacturing, CdTe benefits

from high-throughput deposition techniques such as close-spaced sublimation and vapour transport deposition [52,56], which enable rapid module production. However, continued optimization of these processes is required to further reduce costs while maintaining high efficiency and module reliability.

Future improvements in CdTe solar technology will depend on innovations in alternative materials, new fabrication techniques, and continued advancements in bandgap engineering. These developments will be essential for improving both the PCE and sustainability of CdTe solar cells. By addressing these challenges, CdTe technology can continue to thrive in the global photovoltaic market, maintaining its position as a key player in thin-film solar energy.

2.3. CZTS/CZTSSe

CZTS and CZTSSe are promising thin-film materials for solar cells, known for the abundance of their constituents in the Earth's crust and their non-toxic composition, making them an environmentally friendly alternative to other thin-film technologies such as CIGS and CdTe. Unlike CIGS, which contains rare elements like In and Ga, or CdTe which uses toxic Cd, CZTS/CZTSSe are composed of copper (Cu), zinc (Zn), tin (Sn), and S/Se, offering a more environmentally friendly and sustainable option [22,68–70].

CZTS/CZTSSe shares structural similarities with CIGS, including a tuneable bandgap that ranges from 1.0 eV for $Cu_2ZnSnSe_4$ to approximately 1.5 eV for Cu_2ZnSnS_4, which can be adjusted by varying the S to Se ratio [69–71]. This tuneable bandgap allows optimization of the light absorption profile, making it suitable for both single- and tandem-junction solar cells [69,72]. As with CIGS, this flexibility is essential for maximizing PCE [73]. The kesterite structure of CZTS/CZTSSe, with its tetragonal arrangement and direct bandgap, is highly effective at absorbing light due to its strong alignment with the solar spectrum. Its high absorption coefficient ensures that even thin layers can efficiently capture sunlight, making it well suited for solar energy conversion [69,73,74].

A typical CZTS/CZTSSe solar cell structure consists of multiple layers, each serving a specific function for enhancing performance. The structure typically includes an SLG substrate, followed by a Mo back contact, a CZTS/CZTSSe absorber layer, a CdS buffer layer, a TCO, a metal grid, and an antireflective coating (Figure 5). This layered configuration is crucial for optimal light absorption, charge separation, and carrier transport, ultimately contributing to efficient solar energy conversion.

The fabrication of CZTS/CZTSSe thin films has been explored using various techniques, including sputtering, sol–gel processing, and co-evaporation [68,71,72,74,75]. Each of these methods has its own advantages and drawbacks in terms of cost, scalability, and material quality. Sputtering, for example, allows for precise control over film thickness and composition but may be less cost-effective than solution-based methods like sol–gel processing [72,74,76]. Sol–gel methods are generally more cost-effective and scalable, though achieving uniform, stoichiometric films can be challenging [74,75,77]. Co-evaporation, a vacuum-based technique, provides precise control over stoichiometry and morphology but is more complex and expensive than other methods [71,78].

Since its introduction in 2009 as a potential alternative to CIGS with an initial PCE of 6.7%, significant progress has been made to enhance the PCE of CZTS/CZTSSe-based solar cells (Figure 6). Several approaches to the deposition methods have been attempted, as described in Table 5. In 2011, improved synthesis methods using spin-coating and hydrazine treatment raised the PCE to 10.1%, followed by co-evaporation techniques in 2013, which pulled PCE to 9.15%. By 2019, further advancements in interface and material quality improvements brought PCE to 12.6%, and in 2022, defect engineering and advanced interface strategies helped achieve a record PCE of 13.6%, with the current world record

standing at 14.9% [21,22]. Despite these advancements, CZTS/CZTSSe solar cells have not yet reached the PCE levels of CIGS or CdTe solar cells, which typically operate in the range of 15–20% or higher [21]. Researchers are actively working to optimize fabrication processes, reduce defect densities, and enhance grain boundary passivation [22].

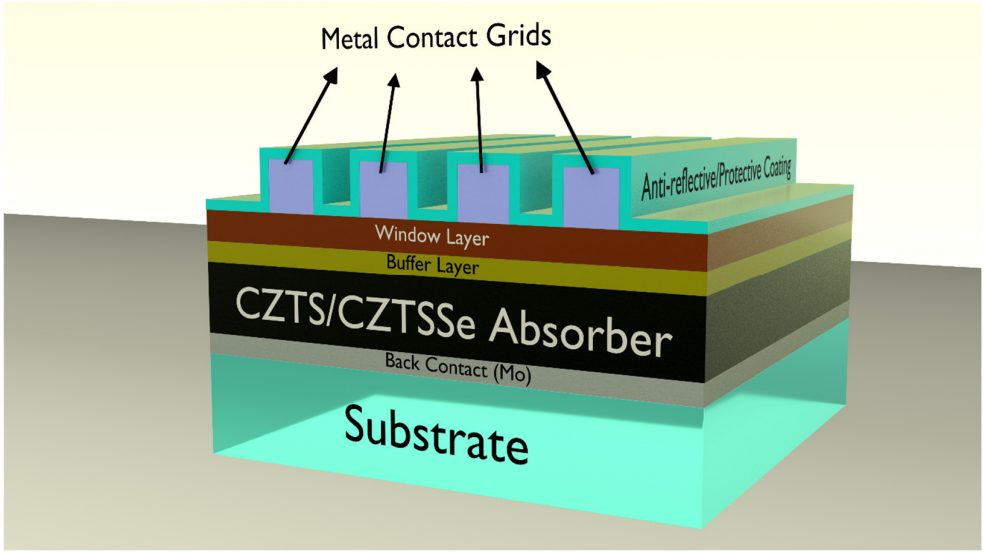

Figure 5. Illustration of the structure of a CZTS/CZTSSe solar cell, depicting its key structural layers: the glass substrate, Mo back contact, CZTS/CZTSSe absorber layer, CdS buffer layer, window, anti-reflective coating, and metal grids.

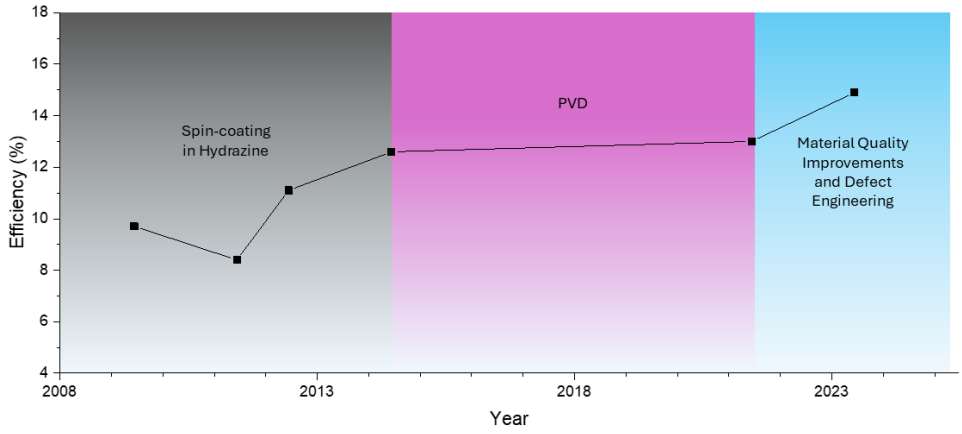

Figure 6. CZTS/CZTSSe solar cell PCE progression showcasing major advancements in deposition techniques, PVD techniques and material quality and defect engineering, leading to a peak PCE of 14.9% (data from research-cell efficiency data NREL).

CZTSSe technology faces significant challenges that have hindered its industrial adoption. One of the primary limitations is its relatively lower efficiency compared to CIGS and CdTe, with record efficiencies still below 15% [21]. High defect densities and complex recombination mechanisms contribute to voltage losses and reduced carrier collection, limiting overall device performance. The defect chemistry of CZTSSe is particularly complex, with the presence of antisite defects and deep-level recombination centres leading to significant V_{oc} deficits [71,79]. Additionally, bandgap fluctuations within the CZTS/CZTSSe absorber layer contribute to poor charge transport and reduced PCE [71,79]. These issues are further exacerbated by high V_{oc} deficits, often caused by antisite defects such as Sn_{Zn} and Cu_{Zn}, as well as secondary phase formation during synthesis, leading to band tailing effects that degrade PCE [73,80].

Achieving optimal band alignment between CZTS/CZTSSe and the buffer layer is also crucial for effective charge carrier separation and collection, highlighting the need for advanced bandgap engineering techniques to improve photovoltaic performance [68]. The fabrication of CZTSSe also presents scalability challenges. The commonly used two-step sulfurization/selenization process requires precise control over precursor composition and annealing conditions to prevent secondary phase formation, which can negatively impact efficiency. While deposition techniques such as sputtering, electrochemical deposition, and solution processing have been explored for CZTSSe manufacturing (Table 5), achieving uniform and high-quality absorber layers at a competitive cost remains a major hurdle.

Despite these challenges, CZTSSe remains an attractive candidate for tandem solar cells due to its bandgap tunability, particularly in applications requiring wide-bandgap absorbers. Addressing these limitations requires ongoing efforts in defect control, compositional optimization, and bandgap engineering. Progress in these areas can significantly improve the performance of CZTS/CZTSSe-based solar cells, paving the way for high-efficiency, sustainable photovoltaic solutions [22,72,73,79]. Continued research in defect passivation, interface engineering, and process optimization is essential to bring CZTSSe closer to industrial viability.

Table 5. Trends in CZTS solar cell efficiencies with various grading strategies and deposition techniques.

Year	CZTS Grading Strategy	V_{oc} (V)	J_{sc} (mA/cm^2)	FF (%)	η (%)	Ref.
2010	Hot injection	0.43	31.2	53.9	7.23	[81]
2010	Spin coating (hydrazine solution-based precursor)	0.516	28.6	65	9.66	[82]
2010	Thermal evaporation	0.499	29.55	64.3	9.5	[83]
2011	Spin coating (hydrazine solution-based precursor)	0.517	30.8	63.7	10.1	[84]
2012	Spin coating (hydrazine solution-based precursor)	0.459	34.5	69.8	11.1	[85]
2013	Solution process	0.505	24.5	57.83	7.17	[86]
2014	Spin coating (hydrazine solution-based precursor)	0.513	35.2	69.8	12.6	[87]
2014	Spin coating	0.52	23.28	49.6	6	[88]
2014	Annealing of metal precursor	0.516	34.1	62.5	11	[89]
2016	Sequential sputtering	0.521	34.98	67.2	12.3	[90]
2016	Compound sputtering	0.61	17.5	–	6	[91]
2016	Doctor-blade pasting	0.621	16.3	50.7	5.1	[92]
2017	Two-step process	0.444	30.9	47.5	6.4	[93]
2017	Two-step process	0.39	33.1	59	7.5	[94]
2017	Doctor-blade pasting	0.617	13.2	49.9	6	[95]
2017	Two-step process	0.615	16.3	50.7	5.1	[96]
2017	Electron beam evaporation	0.744	16	46	5.5	[97]
2018	Two-step sputtering	0.588	22.15	46.9	6.11	[98]
2018	Thermal evaporation	0.655	18.7	57.6	7	[99]
2019	Two-step process	0.621	16.3	50.7	5.1	[100]
2019	Solution process	0.417	36.7	52.27	8.01	[101]
2020	Two-step process	0.617	18	54.1	6	[102]
2021	Two-step process	0.69	17.12	37.15	4.4	[103]

2.4. Economic and Environmental Impacts of TFSCs

2.4.1. Comparison of Production Costs and Economic Returns

The production costs of TFSCs and crystalline silicon solar cells vary significantly due to differences in material usage and manufacturing processes. Crystalline silicon (c-Si) modules require high-purity silicon wafers, which contribute to their higher material and energy costs. The cost of silicon wafers, historically dominant in overall PV

costs, has dropped significantly, but the capital expenditure required for wafer-based PV manufacturing remains high [104].

In contrast, TFSCs use direct deposition techniques, allowing for lower material costs and reduced processing temperatures. CdTe, for instance, requires 98% less semiconductor material than silicon PV and benefits from low-cost, high-throughput manufacturing [65,105]. CIGS manufacturing, however, remains relatively expensive due to the scarcity of indium and gallium [106]. CZTSSe, made from earth-abundant elements, offers the lowest material cost but suffers from lower efficiencies and stability concerns [107,108].

Economic viability is often assessed using the levelized cost of electricity (LCOE). CdTe has one of the lowest LCOEs due to its high efficiency, low material cost, and rapid production scalability, while CIGS LCOE remains higher due to complex deposition and material scarcity [105]. Silicon PV, despite higher manufacturing costs, benefits from economies of scale and longer operational lifetimes, making it the dominant technology in large-scale installations [104].

2.4.2. Environmental Impact and Sustainability

TFSCs generally have a lower environmental footprint than c-Si due to reduced material usage and lower processing temperatures. CdTe modules have the shortest energy payback time (EPBT), at 0.4–1.0 years, followed by CIGS (~1.5 years) and c-Si (2.5–3.5 years), reflecting the higher energy demands of silicon wafer production [65,109].

Recycling strategies vary across technologies. Concerns about Cd toxicity have necessitated stringent recycling programmes. CdTe appears to have well-established industrial recycling programmes [110–114]. First Solar claims that their high-value recycling services recover over 90% of both semi-conductor and glass materials, which helps mitigate environmental risks associated with Cd content [110,111]. First Solar states that they currently operate high-capacity recycling facilities in the USA, Germany, India, Malaysia, and Vietnam, with a combined annual recycling capacity of 88,000 metric tons [110,111]. This infrastructure supports a circular economy by enabling PV technology to be recycled multiple times.

CIGS recycling remains costly though worthwhile due to the high-value scarce elements like indium and gallium [115]. Silicon PV recycling is improving, but silver and other key materials remain difficult to recover economically [66]. In terms of material toxicity, CdTe has raised concerns due to Cd content, though controlled recycling minimizes risks. CIGS presents selenium leaching issues, while CZTSSe is considered the most environmentally benign option [106,107].

2.4.3. Large-Scale Applications and Commercial Deployment

TFSCs have successfully transitioned from research to commercial-scale deployment, with CdTe leading in utility-scale solar farms, accounting for a significant portion of large-scale PV installations. First Solar has achieved >22% efficiency in CdTe modules, making it the most commercially successful TFSC [105].

CIGS excels in flexible and lightweight applications, such as BIPV, aerospace, and portable solar solutions, due to its high efficiency and superior low-light performance. However, high production costs and reliance on scarce materials limit its large-scale use [106]. CZTSSe, though promising due to its earth-abundant composition, remains in early-stage commercialization due to lower efficiency and stability [107].

Recent advancements in perovskite–silicon tandem cells have surpassed 28% efficiency, with Qcells reporting 28.6% for commercial-sized modules, highlighting a promising pathway for next-generation photovoltaics [65].

3. Strategies to Improve TFSC PCE

3.1. CIGS

3.1.1. Bandgap Engineering

Bandgap engineering plays a crucial role in optimizing the performance of TFSCs by tailoring the material's electronic properties to enhance light absorption, improve PCE, and increase device stability. Adjusting the bandgap of the absorber layer directly impacts how much of the solar spectrum the cell can absorb. CIGS allows for tuneable bandgaps by varying the ratio of In to Ga, which improves the absorption of light over a broader range of the spectrum [1,22]. This approach also improves charge carrier transport by reducing recombination losses at grain boundaries and interfaces. Alkali metal treatments (e.g., using Cs or Rb) have further optimized this by passivating defects and enhancing stability [16,116].

Tailoring Bandgaps for Better Spectral Utilization

Tailoring the bandgap of thin-film materials ensures that the solar cell can effectively capture photons from different regions of the solar spectrum. A material with a wide bandgap can absorb high-energy photons, while a lower bandgap material is better suited for capturing photons from the red or infrared regions (Figure 7). By adjusting the bandgap, solar cells can be optimized to maximize power conversion efficiency (PCE) by capturing more photons across a range of wavelengths while maintaining the compromise between efficient photon absorption and effective photogenerated carrier collection [25,117]. For instance, bandgap grading in CIGS cells creates a more favourable energy profile for photon absorption and carrier collection [25].

Approaching the Shockley–Queisser Limit

The Shockley–Queisser limit defines the theoretical maximum PCE of a single-junction solar cell based on its bandgap. By modifying the bandgap through techniques like compositional tuning or PDT, TFSCs can approach this PCE limit [25,116]. While no solar cell can exceed the Shockley–Queisser limit for a single-junction configuration, bandgap engineering enables cells to come closer to this maximum by optimizing photon absorption and minimizing recombination losses [24,118].

Tuning the bandgap is critical for enhancing the PCE of CIGS solar cells. The optimal bandgap for single-junction solar cells is around 1.4–1.5 eV, which closely aligns with the maximum power point predicted by the Shockley–Queisser limit [118]. By adjusting the Ga/In ratio, the CIGS bandgap can be fine-tuned to this optimal range, ensuring maximum photon absorption while minimizing thermalization losses (energy lost as heat) [22,118,119].

For example, for CIGS, increasing the Ga content increases its bandgap, thereby improving its ability to absorb shorter wavelengths, which contributes to higher V_{oc} and improved PCE. This bandgap engineering also enhances charge carrier separation and reduces recombination at grain boundaries, leading to better overall device performance [119,120].

Additionally, graded bandgap profiles, where the bandgap is gradually varied throughout the thickness of the CIGS layer, further optimize the collection of charge carriers. This approach improves the PCE of the device by allowing better charge transport and reducing recombination at the back interface [14,25,117,120].

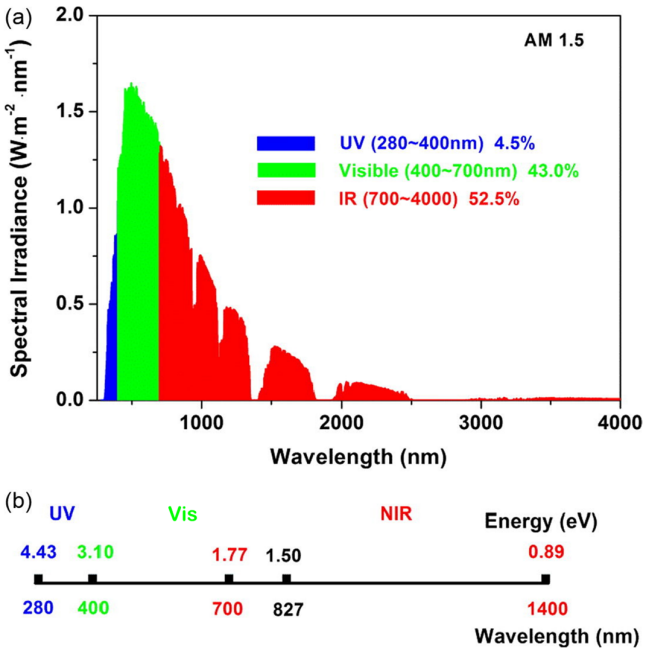

Figure 7. Spectral distribution of solar irradiance under AM 1.5. (**a**) Breakdown of UV (280–400 nm, 4.5%), visible (400–700 nm, 43.0%), and IR (700–4000 nm, 52.5%) contributions. (**b**) Energy ranges for UV, Vis, and NIR regions. Figure reproduced with permission from [119]. Licence number: 5950090939672.

The bandgap E_g of CIGS can be expressed as a function of the Ga content (denoted as x). The empirical relationship is given by

$$E_g = E_{gCIS} + xE_{gCGS} - bx \quad (1)$$

where E_{gCIS} represents the bandgap energy of CIS, and E_{gCGS} corresponds to the bandgap energy of CGS. The parameter b, which ranges from 0.15 to 0.24, accounts for a bending coefficient [24,121]. This empirical formula can be further simplified, allowing the bandgap to be directly calculated from the elemental composition of the pentenary alloy:

$$E_g^{CIGSSe} = 1.00 + 0.13x^2 + 0.08xy + 0.13x + 0.55x + 0.54y \quad (2)$$

where E_g^{CIGSSe} is the bandgap of the $CuIn_{1-x}Ga_x\left(Se_{1-y}S_y\right)_2$ compound, and x and y are the contents of Ga and S in the alloy, respectively [121]. Maximizing the absorption of solar energy requires careful alignment of the bandgap with the solar spectrum. If the bandgap is too low, it can lead to significant thermalization losses, while a bandgap that is too high results in transparency to critical portions of the spectrum [119]. The ability to adjust the bandgap offers the potential for optimization based on environmental factors, such as geographic location and expected irradiance.

In addition to maximizing absorption, there is a critical relationship between V_{oc} and the bandgap. As the bandgap increases, V_{oc} typically rises due to reduced recombination losses, contributing to an overall increase in solar cell PCE [119]. However, this increase must be carefully balanced against short-circuit current density (J_{sc}), which often declines with a higher bandgap because less light is absorbed, particularly in the lower-energy portions of the spectrum [120,122].

Employing bandgap grading, which consists of the variations in the bandgap throughout the thickness of the absorber layer, can lead to an enhanced depletion region within the solar cell [25,123]. These improved depletion regions facilitate the collection of photogenerated carriers. A bandgap gradient can mitigate recombination losses near the surface while

improving photon absorption across a broader wavelength range [25]. By optimizing the bandgap grading, defect states that act as recombination centres are minimized, reducing recombination losses and enhancing solar cell performance [120]. This optimization is critical for improving the PCE of solar cells.

The flexibility of adjusting the bandgap in CIGS solar cells opens up new possibilities for high-performance tandem solar cells. In these configurations, different materials with tailored bandgaps can be stacked to capture a broader spectrum of light. A widened bandgap in CIGS enables effective integration with sub-cells optimized for absorbing lower-energy photons, enhancing the overall PCE of the solar cell system. Similarly, using a narrow bandgap CIGS layer as the bottom sub-cell in a tandem solar cell configuration allows for the capture of longer wavelength photons that pass through the top sub-cell. This approach improves the light-harvesting capability of the tandem device and further boosts its PCE.

Ga Grading and Its Effect on Bandgap Profile

Ga grading in CIGS solar cells is a pivotal method to tailor the bandgap profile, targeting enhancements in both V_{oc} and overall cell PCE. By adjusting the Ga/(Ga + In) ratio, the bandgap of the absorber can be tuned to optimize carrier collection and recombination dynamics [37,124]. However, while higher Ga content increases the bandgap and enhances V_{oc}, excessive Ga incorporation can lead to several challenges. A higher bandgap reduces the absorption coefficient in the near-infrared region, leading to a decline in J_{sc} [25,37,43,124]. Additionally, increased Ga content alters the conduction band position, potentially weakening the built-in electric field, which reduces carrier separation efficiency [25,37,55,123]. Studies have also shown that excessive Ga can introduce defect states and deep-level recombination centres, further limiting overall efficiency [25,43]. To balance V_{oc} gains against J_{sc} losses while minimizing recombination, Ga grading strategies have been developed to optimize the bandgap profile within the CIGS absorber.

By creating a gradient of Ga content within the absorber layer, researchers can manipulate the bandgap to form a "notch" near the CIGS/CdS interface, which reduces recombination losses and facilitates better charge separation and collection. This gradation in Ga concentration effectively increases the energy difference between the conduction band (CB) and valence band (VB), translating to a higher V_{oc} without significantly compromising J_{sc} [125]. Figure 8 illustrates these band diagrams, providing a visual representation of different Ga grading profiles in CIGS absorber layers. It highlights various approaches such as increased Ga concentration at the back contact (Figure 8a), decreased Ga concentration at the back contact (Figure 8b), and more complex double or V-shaped grading structures (Figure 8c,e,f). These profiles illustrate the various possibilities for bandgap grading enabled by bandgap engineering, showcasing how the VB and CB can be tailored to enhance device performance.

Back Grading: In a normal grading profile, the Ga content increases gradually toward the back contact (Mo interface), resulting in a bandgap widening at the rear of the absorber (Figure 8a). This configuration has been widely employed to mitigate back-contact recombination losses and enhance charge collection efficiency. Studies have shown that normal grading creates an electric field that repels photogenerated electrons from the back interface, thereby reducing recombination and improving carrier transport [126]. This effect becomes particularly significant in ultra-thin absorbers (<1 μm), where back-surface recombination is a dominant loss mechanism [124].

However, while normal grading effectively increases V_{oc} by reducing recombination at the Mo/CIGS interface, it can also introduce transport barriers for holes, leading to a reduction in FF if not carefully optimized [37]. Additionally, the bandgap widening at the

back contact reduces absorption in that region, which may slightly limit J_{sc}, especially in cases where light absorption in the near-infrared spectrum is critical [124].

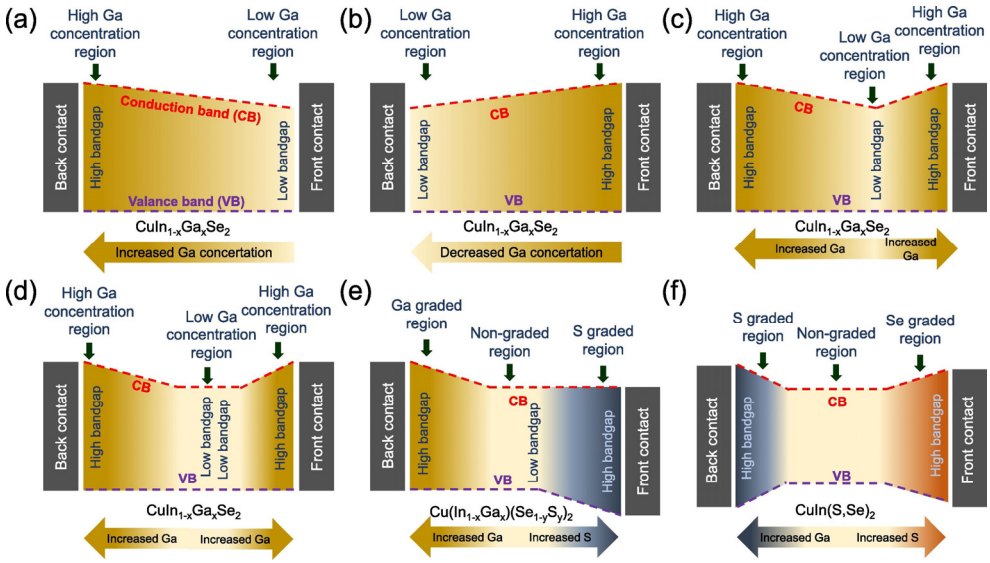

Figure 8. Bandgap engineering strategies for chalcopyrite TFSC: (**a**,**b**) uniform Ga grading, increasing or decreasing towards the back contact; (**c**,**d**) double grading with high Ga concentration at both contacts, with (**d**) featuring an extended low-Ga mid-region; (**e**) double grading of Ga and S in $CuInGa(Se,S)_2$ with VB graded at the front, CB at the back, and a non-graded Se-S transition; and (**f**) $CuIn(S,Se)_2$ absorber with a S-rich surface and Se-rich back for optimal V_{OC} and band alignment. Figure reproduced with permission from [22]. Licence number: 5950091328759.

Front Grading: Front grading involves increasing the Ga concentration toward the front interface (CIGS/buffer interface), leading to a higher bandgap near the junction (Figure 8b). This profile has been shown to reduce interface recombination, thereby enhancing V_{oc} [127]. The resulting built-in electric field can also facilitate charge separation, promoting carrier drift toward the junction and potentially improving charge extraction [128]. Furthermore, reverse grading enhances blue light absorption, which can be beneficial for optimizing the EQE in the shorter wavelength range [37].

Despite these advantages, excessive Ga incorporation at the front interface can create a potential barrier for photogenerated electrons, impeding charge collection and reducing efficiency [128]. Moreover, an excessively high front-surface bandgap can decrease optical absorption in the upper region of the absorber, thereby leading to a lower J_{sc} [127].

Double Grading: A double grading profile is characterized by an increase in Ga content at both the front and back interfaces, with a minimum bandgap located in the middle of the absorber (Figure 8c,d). This configuration aims to combine the advantages of both normal and reverse grading, reducing back-surface recombination while improving interface passivation [126]. The resulting bandgap profile generates two internal electric fields—one near the junction and another at the back contact—which enhance carrier collection and transport efficiency [124].

Device simulations and experimental studies indicate that double grading leads to higher efficiencies compared to single grading strategies, as it offers a balance between V_{oc} and J_{sc} [128]. However, the complexity of precisely controlling the Ga gradient during deposition presents a key fabrication challenge. Furthermore, a stronger bandgap gradient can increase series resistance, potentially impacting FF and overall device performance [22].

Multi-Grading: Multi-grading refers to a more complex Ga distribution, incorporating multiple gradient transitions throughout the absorber (Figure 8e,f). This approach provides greater flexibility in optimizing bandgap tailoring, allowing for enhanced spectral

utilization and charge transport efficiency [124]. By minimizing abrupt bandgap variations, multi-grading can also reduce bandgap fluctuations, which helps to minimize potential barriers for carrier transport and improve overall device stability [22]. Despite its potential advantages, multi-grading further increases fabrication complexity and requires precise process control to ensure the desired Ga distribution is achieved during deposition [37].

Studies by Namnuan and Chatraphorn illustrate the application of Ga grading in a three-stage co-evaporation process. By modulating the Ga content across deposition stages, they achieved a pronounced bandgap profile notch (Figure 8d) that enhanced V_{oc} to 698.4 mV and increased the cell PCE to 17.61%. This controlled profile minimized recombination at the junction, maintaining J_{sc} by enhancing charge collection, critical in maximizing PCE [2]. Similarly, Gohri et al. analyzed the impact of multiple Ga grading profiles and found that a double grading structure, with a lower Ga concentration near the surface and a higher Ga concentration near the back contact (modified version of Figure 8c), yielded the best results in minimizing recombination while retaining strong absorption characteristics, thus optimizing both V_{oc} and J_{sc} [123].

Yan et al. explored an alternative method by modifying the Cu deposition pattern in the three-stage co-evaporation, extending the GGI $(Ga/(Ga + In))$ notch profile near the surface (Figure 8d). This broader GGI notch led to an approximately 10% increase in J_{sc} and an improvement of 32.6% over their initial efficiency of 13.8%, reaching 18.3% PCE in flexible CIGS devices. This approach is particularly valuable for the low-temperature manufacturing of flexible CIGS, as it allows for substantial PCE improvements without requiring the high temperatures that rigid substrates can tolerate [129]. Moreover, Xin et al. employed a grain boundary migration-driven diffusion mechanism for Ga within CIGS films prepared using magnetron sputtering from a quaternary target, achieving a V-shaped bandgap that elevated V_{oc} from 405 mV to 515 mV. This configuration leveraged Ga's controlled diffusion to optimize carrier transport, highlighting the importance of maintaining precise Ga control during annealing to enhance device performance [130].

In the study by Wang et al., a pulsed optic-thermal annealing method was used to address Ga aggregation at grain boundaries, a common issue in CIGS films deposited by the electrodeposition method, which contributes to recombination and diminishes V_{oc}. Their pulsed annealing approach facilitated better Ga distribution and crystallinity, leading to a PCE increase to 9.14%. This method highlights how advanced thermal processing techniques can complement Ga grading to optimize the bandgap profile and improve cell PCE [131].

Furthermore, advanced computational models have supported these empirical findings by providing predictive insights into the optimal Ga distribution for enhancing both V_{oc} and J_{sc}. Deo et al. used simulations to investigate the effects of varying Ga gradients in CIGS absorber layers, demonstrating that an optimized Ga gradient, with a composition range of 0.32–0.28 (Ga/(Ga + In)), effectively reduces recombination losses by grading the bandgap (E_g: 1.19–1.17 eV) and electron affinity (χ_e: 4.24–4.28 eV). This optimization is critical for enhancing device performance, particularly under variable light conditions [132].

Al Alloying

Al alloying in CIGS solar cells is a promising approach to increase the bandgap of the absorber layer while maintaining desirable efficiency characteristics, offering an alternative to simply adjusting the Ga and In ratio. Increasing the Ga content in CIGS beyond a certain point (typically Ga/(In + Ga) > 0.3) leads to efficiency losses due to higher defect density and increased interface recombination, which negatively impacts the V_{oc} and PCE. Al doping, on the other hand, allows for a more effective increase in the bandgap while mitigating some of these issues. Al atoms are smaller than Ga and can substitute

In more easily, leading to improved lattice stability and fewer defects, thereby avoiding the recombination issues typically observed with high Ga content. With a higher intrinsic bandgap of 2.7 eV for $CuAlSe_2$, Al allows more flexibility in bandgap tuning for better matching with the solar spectrum, which is critical for enhancing PCE [133–135].

However, incorporating Al into CIGS also presents certain challenges that must be addressed to optimize device performance. One of the primary issues with Al doping is achieving a uniform distribution of Al throughout the CIGAS films. Al tends to accumulate in specific regions, such as near the middle or at the surface, leading to compositional inhomogeneity. PDT is often required to redistribute Al more uniformly, which increases fabrication complexity and time. Furthermore, the presence of Al tends to reduce the grain size of the films, which can elevate the recombination rates at grain boundaries and negatively affect the efficiency of charge carrier transport. This effect of reduced grain size also contributes to increased surface roughness, potentially impacting light absorption and thereby limiting efficiency. Al's high reactivity can also make it challenging to prevent the formation of undesirable secondary phases, such as Al_2Se_3, which can negatively affect the device properties if deposition conditions are not strictly controlled [133,134,136]. Effective implementation requires the careful optimization of deposition conditions to achieve a uniform distribution of Al, maintain larger grain sizes, and prevent unwanted secondary phases, ensuring that the potential benefits of Al doping are fully realized without introducing new inefficiencies.

3.1.2. Alkali Doping

Recent advances in CIGS solar cells have increasingly focused on bandgap tuning and PCE improvements through selective doping with alkali metals. Traditional enhancements achieved by Na diffusion from SLG substrates have led to significant improvements in V_{oc} and fill factor (FF) through grain boundary passivation and conductivity increases within the CIGS absorber. However, in recent years, research has expanded to investigate additional elements, including heavy alkaline elements like Caesium (Cs) and Rubidium (Rb), which show potential to further optimize these properties by fine-tuning the electronic, structural, and optical characteristics of CIGS solar cells.

Na as a Foundational Dopant

Na has been a cornerstone of CIGS solar cell enhancement due to its unique interactions at grain boundaries and within the bulk CIGS matrix. Na incorporation is associated with the passivation of defects, such as vacancies and antisite defects, which form during film growth. Na also plays a crucial role at the grain boundaries of CIGS absorbers. Studies have shown that Na preferentially segregates at grain boundaries (Figure 9), where it effectively passivates defect states that would otherwise act as recombination centres [137,138]. This passivation effect increases the hole concentration, thereby enhancing p-type conductivity, and reducing the density of nonradiative recombination centres [139]. Notably, Na doping forms Na-In and Na-Ga defects within the CIGS lattice, which have been shown to increase the electronic potential at grain boundaries, repelling electrons and thereby mitigating recombination pathways. Studies indicate that controlled Na doping can improve V_{oc} by approximately 20% and enhance overall PCE by nearly 50% [3,11,116].

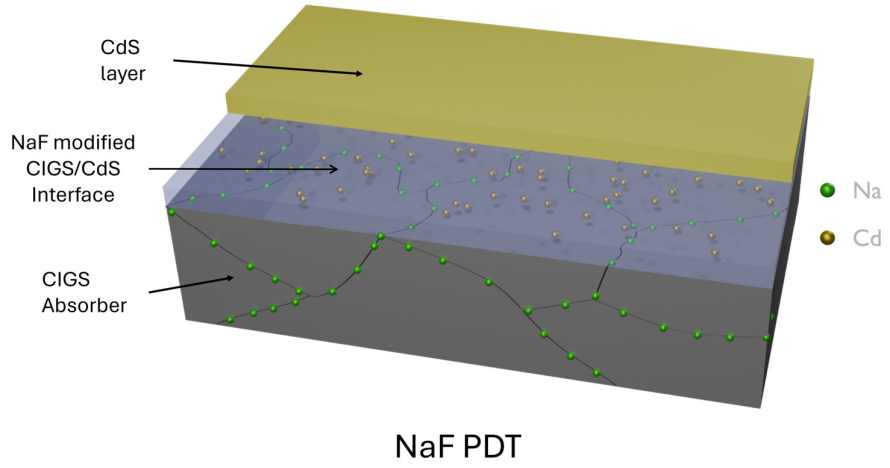

Figure 9. Schematic showing Na segregation at the grain boundaries of CIGS, leading to defect passivation. Na atoms (green) accumulate at grain boundaries, reducing recombination and enhancing the efficiency of the CIGS absorber.

Potassium (K) as a Complementary Dopant

Following Na, K has been a critical dopant for CIGS, often applied through PDT with KF. The larger ionic radius of K compared to Na leads to its preferential incorporation at grain boundaries rather than within grains (Figure 10). This selective placement promotes anisotropic charge transport, improving in-plane resistance and decreasing cell-to-module (CTM) efficiency losses in monolithic modules [11].

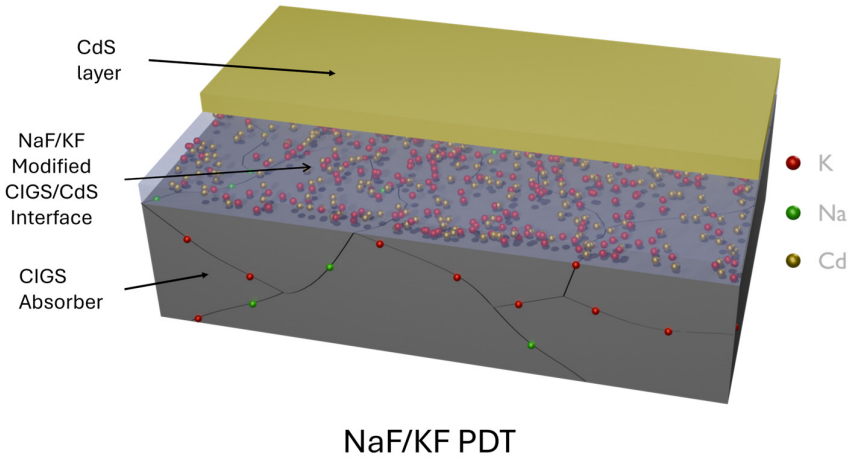

Figure 10. Schematic showing K (red) distribution in CIGS, predominantly at grain boundaries due to its larger ionic radius compared to Na (green).

Furthermore, K doping can widen the depletion region, which improves charge separation efficiency and enhances V_{oc}. As indicated in Figure 10, the increased grain boundary concentration of K contributes to higher grain boundary potential barriers, which are effective in reducing electron–hole recombination. Empirical studies have documented that the KF-PDT can raise the FF and J_{sc}, particularly in large-area devices where current shunting at laser-scribed boundaries is a concern [116,140,141]. This effect is also reflected in the decreased recombination pathways, visible in the diagram as fewer direct paths between carriers, emphasizing how K helps mitigate shunting losses.

Cs Doping

Cs, as a heavy alkali metal, has gained attention due to its impact on bandgap widening. As illustrated in Figure 11b,c, Cs incorporation, particularly through CsF PDT, leads to

notable changes in the grain boundary and grain interior of CIGS thin films. Studies demonstrate that Cs can raise the surface bandgap by forming Cs-compound layers, which mitigate carrier recombination near the surface. This is visible in the new phase formation and ion exchange processes highlighted in Figure 11. Cs incorporation, especially through CsF-PDT, has led to PCE improvements above 18% in CIGS modules, as it forms a more significant injection-blocking layer that suppresses recombination at the front junction and enhances electron transport properties [10,142]. Additionally, Cs also contributes to grain structure refinement, as depicted by the changes in grain boundary and grain interior, reducing the tendency for shunt paths and enhancing the mechanical integrity of thin films under varied operating conditions [142–144].

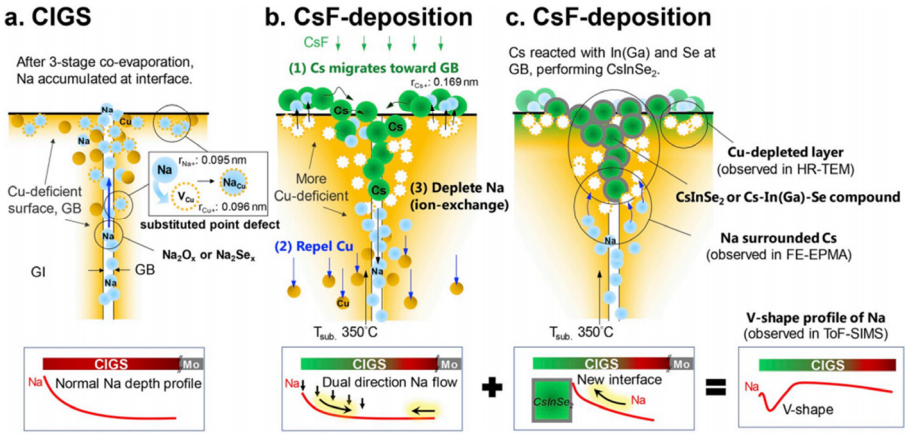

Figure 11. Illustrations of a CIGS thin film showing a 3-stage process: (**a**) without CsF deposition, where Na accumulates at the grain boundary and interface; (**b**,**c**) with CsF deposition at 350 °C, leading to Cs migration, Na depletion, and new Cs-containing phases. Figure reproduced with permission from [143]. Licence number: 5950100035421.

Rb Doping

Rb doping in CIGS solar cells has been explored primarily for its role in reducing grain boundary recombination and stabilizing the absorber structure against radiation-induced damage, making it suitable for space applications. RbF PDT significantly impacts the distribution of alkali elements within the CIGS films, particularly by forming beneficial Rb-Cu complexes that passivate grain boundaries.

RbF-PDT lowers defect densities and enhances V_{oc} through the effective passivation of deep traps within the CIGS absorber, a phenomenon that has been extensively noted in the literature for its contributions to improved PV performance [16,116,145]. Rb is introduced through RbF-PDT, forming Rb-Cu complexes that effectively reduce grain boundary recombination. The subsequent ammonia treatment facilitates a redistribution of both Na and Rb, enhancing the uniformity and passivation at grain boundaries, which ultimately benefits the electrical properties of the absorber by mitigating recombination pathways that affect V_{oc} and FF [116].

Rb doping is especially impactful in Cu-rich CIGS configurations, as it increases the minority carrier lifetime by mitigating non-radiative recombination [16,116,145]. The ion-exchange process during RbF-PDT results in Rb replacing Na at the grain boundaries, pushing Na towards the grain interior. This redistribution reduces defect states, increases carrier concentration, and significantly enhances PV performance [116]. Additionally, it has been found that the presence of heavier alkali metals such as Rb and Cs in the PDT leads to improved device performance compared to lighter alkali metals, attributed to their superior ability to passivate defects and modify surface and grain boundary properties [16,116,145].

The dual role of Rb, passivating grain boundary defects while enhancing carrier concentration in the grain interior, makes RbF-PDT a highly effective method for boosting both the PCE and stability of CIGS solar cells. This is especially advantageous for applications requiring resilience against radiation, such as in space technology. Furthermore, recent research points to the added benefit of reduced Urbach energy and improved microstructural properties of the CIGS absorber when treated with RbF, indicating a reduction in bulk recombination near crystallographic defects [116]. These improvements make RbF-PDT an essential process in advancing CIGS solar cell technology.

3.1.3. Ag Alloying in CIGS

Ag alloying in CIGS solar cells has recently emerged as a promising strategy to enhance both material properties and PV performance. By substituting Cu with Ag, the formation of (Ag,Cu)(In,Ga)Se_2 (ACIGS) introduces key advantages, including improved crystallinity, reduced defect density, and better charge carrier mobility. Ag incorporation has been shown to lower the melting point during film deposition, facilitating the formation of larger grains and reducing grain boundary defects, which act as recombination centres [146]. These effects are particularly beneficial for TFSC, where recombination losses and material quality are critical to achieving high PCE. The resulting ACIGS has demonstrated PCEs exceeding 20%, comparable to conventional silicon solar cells [147,148].

ACIGS technology is well suited for flexible and tandem solar applications due to its tuneable bandgap and improved thermal stability. The lower vapour pressure of Ag compared to Cu allows for more precise control during deposition, reducing unwanted evaporation and enhancing the stability of the material [147,148].

Bandgap Tuning Through Ag Incorporation

Ag alloying in CIGS not only improves crystallinity but also enables precise bandgap tuning. Ag incorporation modifies the electronic structure of the material, leading to slight shifts in the CB and VB edges. This allows for fine-tuning of the bandgap, typically within the range of 1.1 eV to 1.5 eV, making ACIGS suitable for single-junction and tandem applications [148,149].

Experimental evidence shows that Ag incorporation leads to significant improvements in PV performance. For example, solution-processed CIGS solar cells with Ag doping have achieved PCEs of 16.48%, with a V_{oc} of 662 mV and an FF of 75.8% (Figure 12), which is a notable improvement over undoped CIGS cells [150]. The enhancement in external quantum efficiency (EQE) across the visible spectrum and the reduction in Urbach energy from 30.3 meV to 27.3 meV due to Ag incorporation show the reduced band tailing and improved optical quality of the absorber [150].

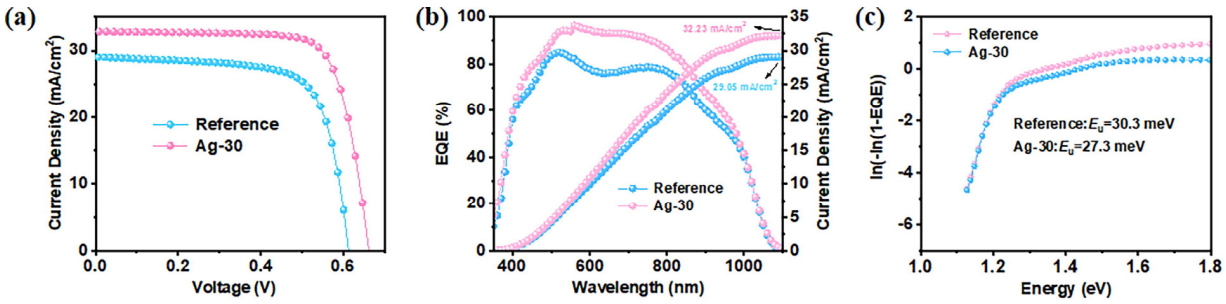

Figure 12. Comparison of the reference and Ag-containing (Ag-30) solution-processed CIGS solar cells. (**a**) J-V curves illustrating the improved performance for Ag-30, achieving higher J_{sc} and V_{oc}. (**b**) EQE curves showing an enhancement in photoresponse across the visible spectrum for Ag-30. (**c**) Extraction of the Urbach energy (E_u) from the EQE spectra indicates a reduction in band tailing for Ag-30. Figure reproduced with permission from [150]. Licence number: 5950100503678.

Similarly, vacuum-based deposition methods have delivered PCEs exceeding 20% when Ag is introduced [23,147,148]. Notably, the current record-holding device, as reported by Keller et al., achieved a certified PCE of 23.64% through high-concentration Ag alloying and a tailored "hockey stick" Ga profile (Figure 13). This device, with a V_{oc} of 767 mV and an FF of 80.5%, also showed significant improvement in its EQE, particularly in the near-infrared region, reflecting effective light absorption and carrier collection. Additionally, the photoluminescence (PL) signal was stronger for the Ag-alloyed device, indicating reduced non-radiative recombination and better crystallinity [23]. These gains in PCE are mainly due to the enhancement of film quality induced by Ag, which reduces recombination losses and improves charge transport properties [23,150].

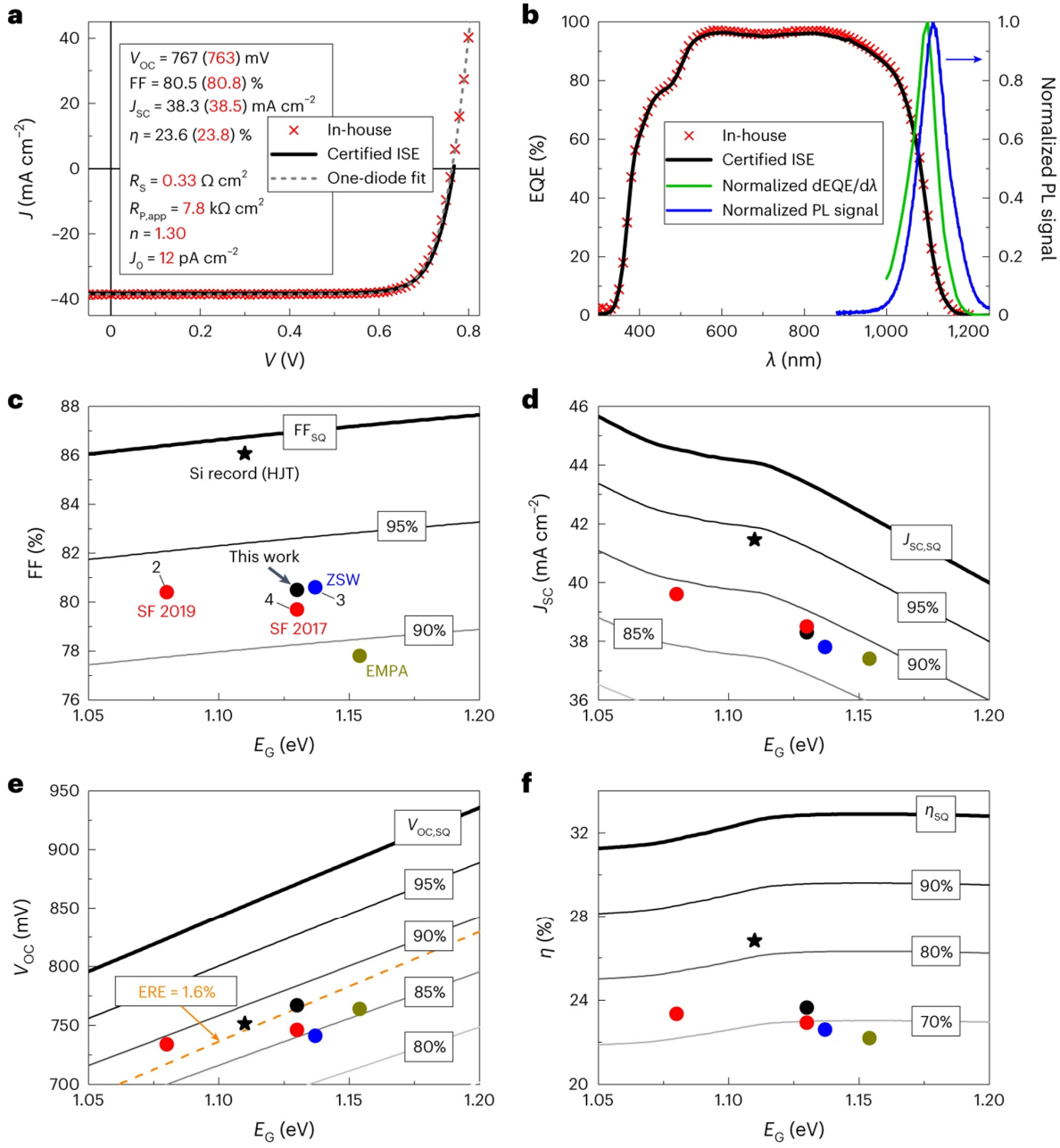

Figure 13. (**a**) J–V characteristics of the record ACIGS solar cell, showing in-house and Fraunhofer Institute for Solar Energy Systems-certified measurements. Key parameters are listed in the inset. (**b**) EQE spectra of the device with normalized $dEQE/d\lambda$ and PL signals. (**c**–**f**) Device metrics, including FF, J_{sc}, V_{oc}, and PCE, were compared with the literature data and a silicon HJT cell. The dashed line in (**e**) shows the predicted V_{oc} trend for an external radiative efficiency of 1.6%. Figure reproduced from [23].

Bandgap tuning through controlled Ag and Ga distribution is particularly important in multi-junction solar cells. A graded bandgap structure, achieved by modulating the Ag-Ga ratio, allows for optimized photon absorption across the solar spectrum. This graded structure can be used in tandem cells, where the top cell must have a wider bandgap (1.4–1.7 eV) to efficiently absorb high-energy photons, while the bottom cell captures lower-energy photons (1.0–1.2 eV) [148,151,152]. By carefully controlling the Ag content, the bandgap of ACIGS can be adjusted to achieve an ideal match between the top and bottom cells in a tandem configuration. This enables each sub-cell to operate at its optimal efficiency, reducing thermalization losses and ensuring better utilization of the solar spectrum, ultimately leading to higher overall PCE.

Enhancement in Solar Cell V_{oc} and FF

Ag incorporation has been consistently shown to enhance key performance parameters in CIGS solar cells, notably V_{oc} and FF. These two parameters directly influence the overall PCE of the solar cell. The improvements in V_{oc} and FF are attributed to the beneficial effects of Ag on both bulk material quality and interface properties, leading to enhanced electronic characteristics.

Yao et al. [149] reported that ACIGS solar cells exhibited a higher V_{oc} of 806 mV, compared to 772 mV for Ag-free cells (Figure 14a,b). This significant improvement is primarily due to the reduction in bulk and interface recombination, facilitated by Ag passivation. Ag helps reduce deep-level defects, improving the quality of the material and reducing recombination losses. As a result, Ag-alloyed devices often achieve V_{oc} values exceeding 600 mV, as reported by other studies [23,148].

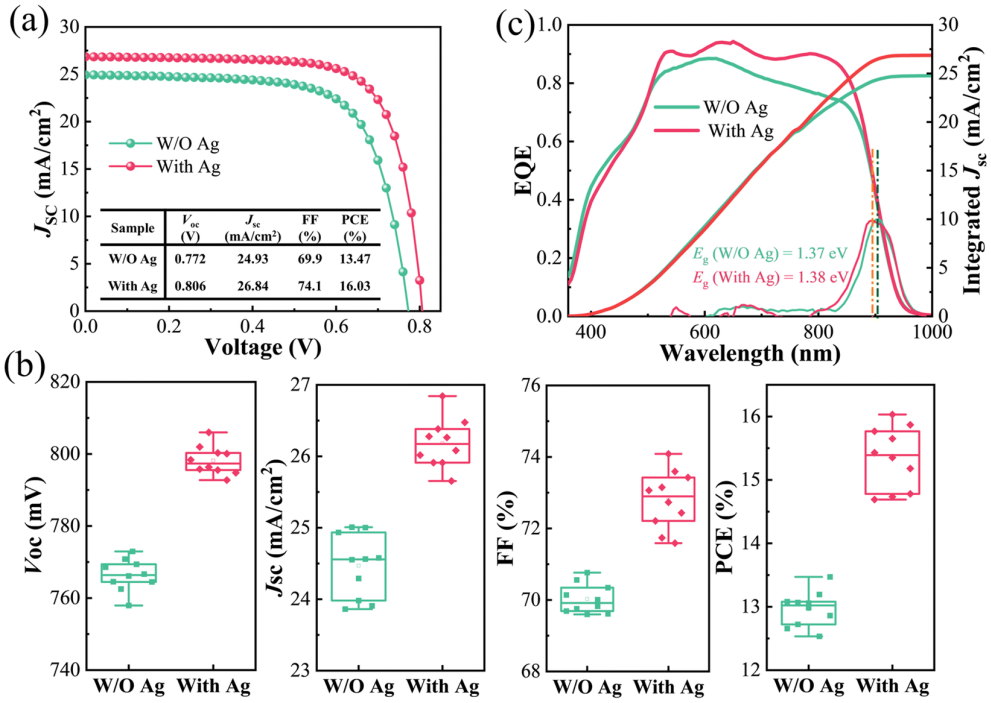

Figure 14. Device performance of CIGS with and without Ag doping: (**a**) current density–voltage (J-V) characteristics under AM 1.5G spectrum, (**b**) statistical distribution of J-V parameters (V_{oc}, J_{sc}, FF, and PCE), indicating improved device performance metrics with Ag incorporation, and (**c**) EQE spectra and integrated J_{sc}, highlighting increased carrier collection efficiency in Ag-containing devices. Figure reproduced with permission from [149]. Licence ID: 1567082-1.

Similarly, the incorporation of Ag also benefits the FF. In the study by Yao et al. [149], the FF increased from 69.9% in the Ag-free device to 74.1% in the Ag-containing device

(Figure 14b). This enhancement indicates improved charge collection efficiency and a reduction in recombination losses, both of which are direct effects of the improvements in material quality and interface properties induced by Ag alloying. In fact, the enhanced crystallinity and reduction in defects of Ag-incorporated materials have led to FF values surpassing 75% in some cases [23,148].

The widening of the space charge region (SCR) due to Ag doping also contributes to these performance enhancements. By extending the SCR, Ag facilitates more effective charge carrier collection, thereby reducing recombination losses. This improvement ensures that a greater proportion of photogenerated carriers contribute to the overall current output, further boosting the FF and overall PCE of Ag-alloyed CIGS solar cells [146].

Impact of Ag on Crystallinity, Defect Reduction, and Grain Growth

Ag alloying significantly improves the crystallinity and grain growth of CIGS films, which is crucial for device performance. Ag incorporation lowers the melting point of the compound, thereby increasing atomic mobility during deposition. This facilitates the growth of larger grains, resulting in fewer grain boundaries and a corresponding reduction in charge carrier recombination [146]. As reported by Yao et al., this effect is further validated by the X-ray diffraction (XRD) analysis, which shows that Ag incorporation results in a distinct preferential growth along the (112) plane, attributed to enhanced crystallization dynamics facilitated by the reduced lattice energy (Figure 15a–c,g,k) [149]. The preferential orientation along the (112) plane is favourable as it minimizes surface energy, ultimately enhancing the film quality and reducing recombination losses.

Grain boundaries are known to act as recombination sites, and their reduction through larger grain formation enhances carrier mobility and reduces recombination losses [146]. The scanning electron microscopy (SEM) images demonstrate that Ag-alloyed CIGS films exhibit fewer grain boundaries and larger grains compared to films without Ag (Figure 15d–f,h–j), which correlates with improved carrier collection efficiency and reduced recombination losses, as indicated by the transient photovoltage (TPV) and transient photocurrent (TPC) decay spectra (Figure 16d,e) [149]. Specifically, the Ag-containing device shows an increased carrier lifetime (522 µs versus 314 µs for the sample not containing any Ag) and more efficient carrier extraction due to the larger grains formed (Figure 16d) [149].

In addition to promoting grain growth, Ag doping significantly reduces nonradiative recombination losses caused by vacancies and energetically deeper antisite defects (e.g., Ga_{Cu}, In_{Cu}), which are common challenges in high-Ga content absorbers. By passivating these defects, particularly at grain boundaries, Ag improves the microstructure of the chalcopyrite films and minimizes electronic and structural disorders, thereby enhancing the overall film quality and device performance [149,151]. PL and time-resolved photoluminescence (TRPL) results corroborate this, with Ag-containing samples exhibiting a higher PL intensity and longer carrier lifetime compared to samples without any Ag (Figure 16a,b) [149]. The increased PL intensity is indicative of a reduction in non-radiative recombination due to fewer defect states, which aligns with Urbach energy measurements showing a decrease from 33.3 meV to 28.6 meV for samples containing Ag, indicating reduced band tailing and defect density (Figure 16c) [149].

This defect passivation improves both the J_{sc} and the FF, contributing to higher overall device PCE [149,151]. Enhanced electrical performance is also illustrated by the EQE spectra, which show an increased response for the Ag-containing sample in the wavelength range of 500–900 nm (Figure 14c) [149].

Recombination losses, which occur when photogenerated charge carriers recombine before reaching the electrodes, are a major challenge in CIGS solar cells. Ag has been shown to mitigate these losses through two key mechanisms: defect reduction and the

widening of the SCR [23,149,151]. By reducing the grain boundaries and the density of deep-level defects, Ag minimizes the number of recombination sites, thus extending carrier lifetimes and improving PCE. This is demonstrated by Yao et al., with the V_{oc} versus light intensity plot, where Ag incorporation led to a lower slope of 1.67 kT/q (where k is the Boltzmann constant, T is the temperature in Kelvin, and q is the elementary charge) compared to 1.92 kT/q for the sample not containing any Ag, indicating reduced defect-assisted recombination (Figure 16f) [149].

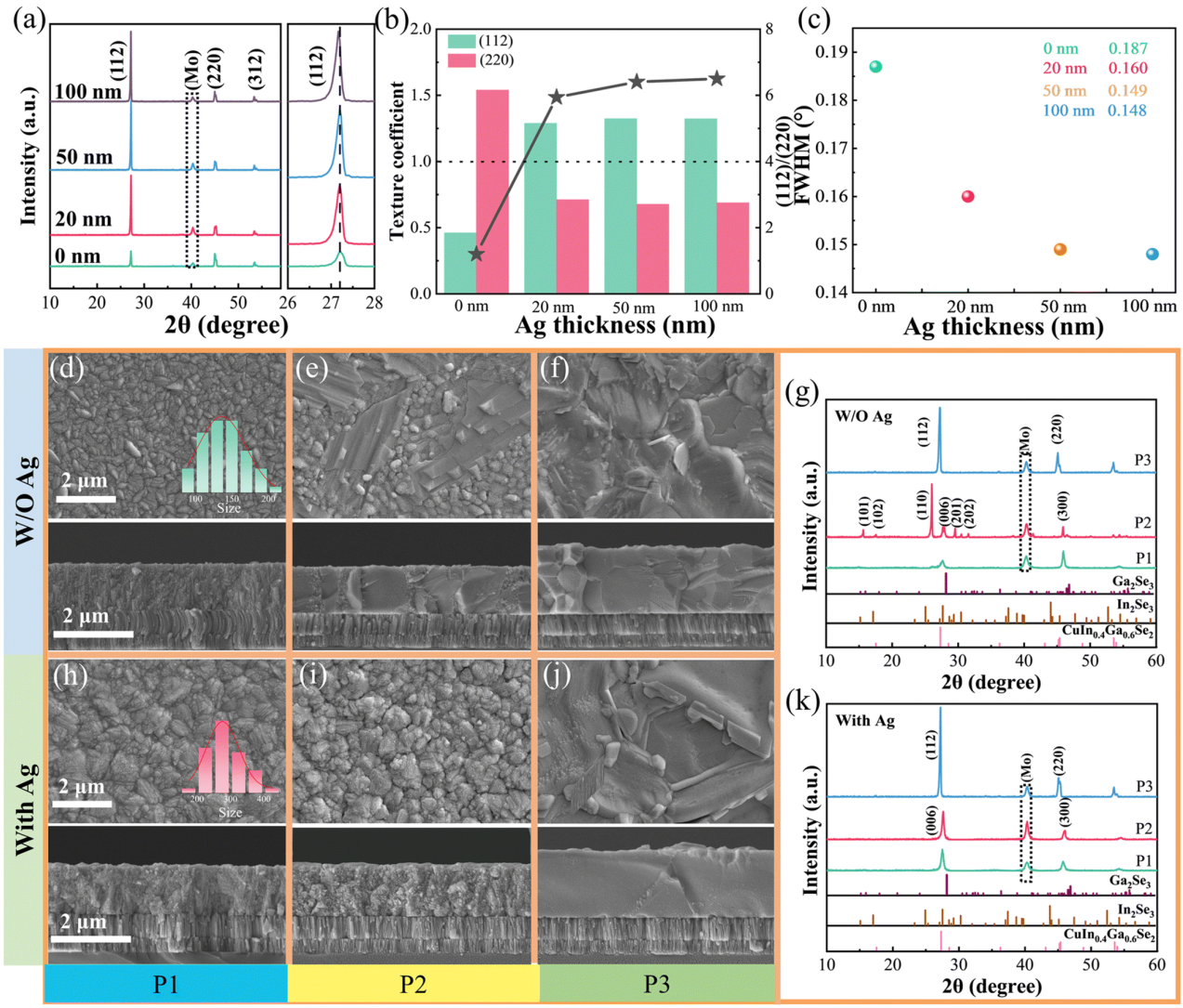

Figure 15. XRD analysis and SEM images showing the impact of Ag doping on the crystallization dynamics of wide-bandgap CIGS films. (**a**) XRD patterns show enhanced preferential growth along the (112) plane for samples containing Ag. (**b**) Texture coefficients of selected (hkl) planes and (**c**) Full Width at Half Maximum (FWHM) values demonstrate improved film quality and reduced defect density with Ag. (**d**–**f**,**h**–**j**) SEM images showing grain growth progression in CIGS samples without and with Ag during different deposition stages, where larger grain sizes are observed in films with Ag. (**g**,**k**) XRD results at different evaporation stages confirming preferential growth orientation. Figure reproduced with permission from [149]. Licence ID: 1567082-1.

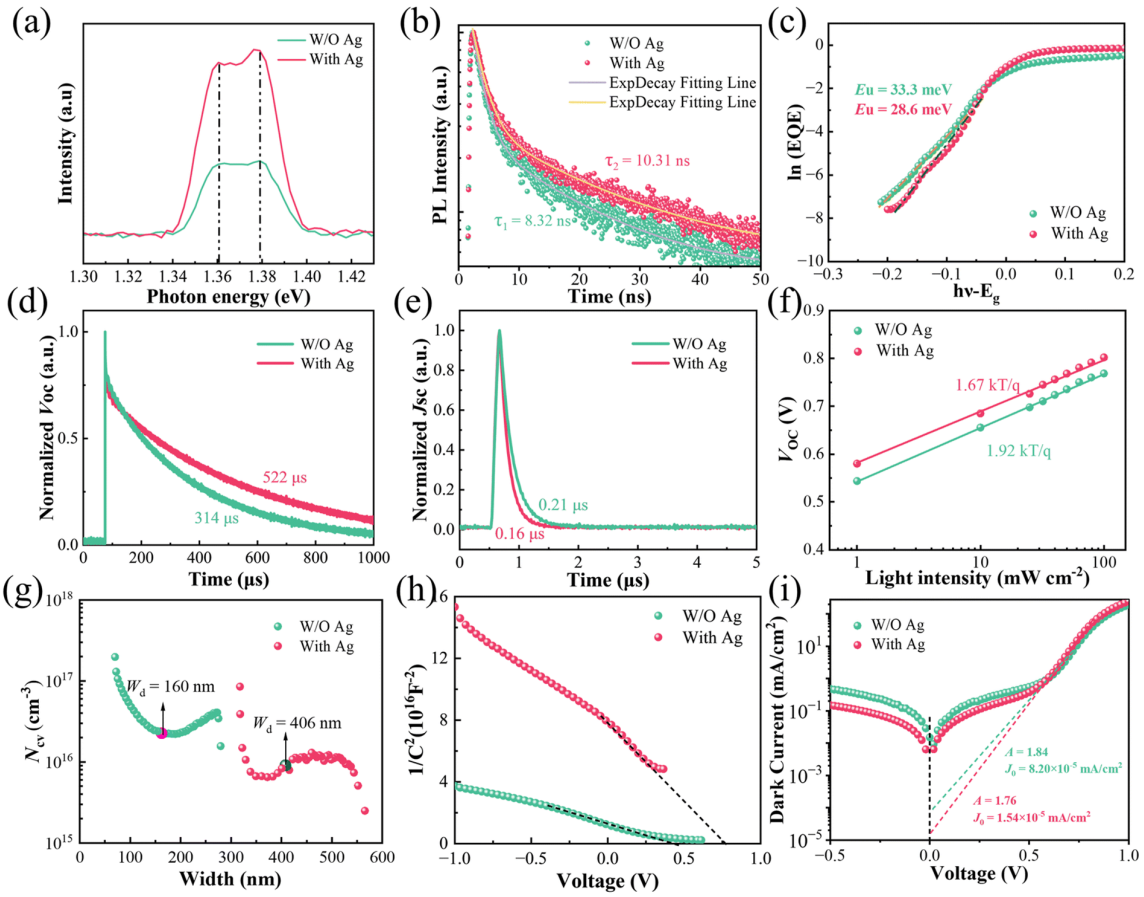

Figure 16. Comparative analysis of wide-bandgap CIGS solar cells with and without Ag pre-deposition. (**a**) PL spectra indicating enhanced carrier recombination in samples containing Ag. (**b**) TRPL highlighting improved minority carrier lifetime with Ag. (**c**) Urbach energy derived from EQE spectra, demonstrating reduced defect states with Ag. (**d**) TPV measurements show increased carrier lifetime. (**e**) TPC indicates faster carrier extraction in Ag-containing cells. (**f**) Dependence of V_{oc} on the light intensity, illustrating reduced defect-assisted recombination with Ag. (**g**) C-V profiling revealed increased depletion width. (**h**) The $1/C^2$ vs. voltage analysis for determining built-in potential. (**i**) Dark current measurements highlight reduced recombination losses in Ag-containing cells, contributing to enhanced device performance. Figure reproduced with permission from [149]. Licence ID: 1567082-1.

Additionally, Ag alloying reduces the carrier concentration, which in turn increases the width of the SCR, which improves the separation of photogenerated electron–hole pairs and enhances carrier collection efficiency [146,149,150]. Capacitance–voltage (C-V) measurements by Yao et al. showed a reduction in the charge carrier concentration from 2.29×10^{16} to 9.89×10^{15}, which further indicates that the depletion width increased from 160 nm to 406 nm in Ag-alloyed films, which directly contributes to improved carrier separation and collection efficiency (Figure 16g) [149]. This results in higher V_{oc} and improved FF, both of which contribute to the overall performance enhancement of ACIGS solar cells [23,148,150]. The reduced saturation current density and ideality factor (A), as observed from the dark current characteristics, further confirm the reduction in recombination losses and enhancement of overall carrier transport properties in Ag-alloyed devices (Figure 16i) [149].

Trade-Offs in Lattice Mismatch and Defect Formation

Despite its advantages, Ag incorporation in CIGS solar cells presents several challenges, particularly in managing lattice mismatch and defect formation. The atomic size

difference between Ag and Cu can introduce strain within the crystal lattice, leading to lattice distortions or dislocations, which can increase recombination rates and reduce overall PCE [149,151]. Furthermore, excessive Ag incorporation can result in phase segregation and secondary phase formation, such as of Ag_2Se, which degrade the properties of the absorber layer [148,151].

In addition, high levels of Ag can increase the risk of ordered vacancy compounds being formed, which act as recombination centres and negatively impact J_{sc} [153,154]. Careful control of the Ag concentration is, therefore, necessary to balance the benefits of Ag alloying with the risks of defect formation and phase separation.

3.1.4. Computational Models Predicting Optimal Doping Profiles

Computational modelling has played an essential role in guiding experimental efforts, particularly for multi-element doping strategies in CIGS cells. Using a Silvaco–Atlas 2D simulator, Zouache et al. compared single- and triple-junction CGS/CIGS structures, finding that carefully controlled Ga and Na distributions optimize current matching across junctions. Their simulations showed a theoretical PCE of up to 33.27% at current-matching points for triple-junction CGS/CIGS cells, highlighting the impact of precisely controlled doping profiles on PCE [155].

Further computational studies by Mabvuer et al. predicted that K and Na dopants could improve grain boundary passivation and band alignment when integrated into specific layers of CIGS multi-junction cells. Their models indicated that Na optimizes the CB, while K enhances electron mobility within the grain boundaries, collectively improving both J_{sc} and V_{oc} without incurring additional fabrication costs [122].

Boukortt et al. used density functional theory (DFT) calculations to simulate how doping with trace amounts of Na and K could reduce interface defects in ultrathin CIGS cells. Their findings revealed that Na and K create a slight bandgap widening that mitigates recombination at the buffer/absorber interface, resulting in significant improvements in quantum efficiency and cell longevity [120].

3.2. CdTe

3.2.1. Bandgap Engineering

CdTe is a prominent thin-film material widely recognized for its near-ideal bandgap of approximately 1.5 eV, which is well aligned with the solar spectrum and conducive to high PCE. This bandgap of CdTe brings it closer to the peak of the Shockley–Queisser efficiency limit, making it highly suitable for solar energy applications. In recent years, considerable progress has been made in CdTe solar cell technology, yielding a PCE over 22%, a notable achievement attributed to advances in materials engineering, interface optimization, and alloying techniques [156,157].

Despite its inherent advantages, CdTe's performance is still below the theoretical maximum, partly due to the limitations imposed by intrinsic material properties and interface recombination losses. Recent research has focused on enhancing CdTe's properties through alloying and doping to achieve higher V_{oc}, reducing sub-bandgap losses, and improving carrier collection, which could further boost PCE towards the 30% threshold [52,54,158].

Using Se for Bandgap Tuning

The alloying of CdTe with Se to form $CdTe_{(1-x)}Se_{(x)}$ has proven to be a versatile and effective strategy for tuning the material's bandgap, thereby extending its absorption capabilities deeper into the infrared spectrum. Zheng et al. showed that the EQE of the CdSeTe/CdTe device is significantly higher across a broader wavelength range compared to the CdTe-only device (Figure 17b), indicating the advantage of this alloying strategy in enhancing infrared absorption. CdSe, with its lower bandgap (1.1 eV compared to

1.5 eV for CdTe), allows for a graded bandgap profile across the CdTe absorber layer when alloyed. This bandgap grading is highly beneficial for increasing the J_{sc}, as it enables the solar cell to capture a broader range of the solar spectrum, particularly in the near-infrared range, where CdTe absorption is otherwise limited [159,160]. This effect is further evidenced by the light J-V characteristics in Figure 17a, where the CdSeTe/CdTe device shows higher current density compared to the CdTe-only device. Additionally, the PL decay data (Figure 17c) reveal a longer carrier lifetime for the CdSeTe/CdTe device, suggesting reduced recombination losses and enhanced carrier collection, contributing to improved overall device performance [159,160].

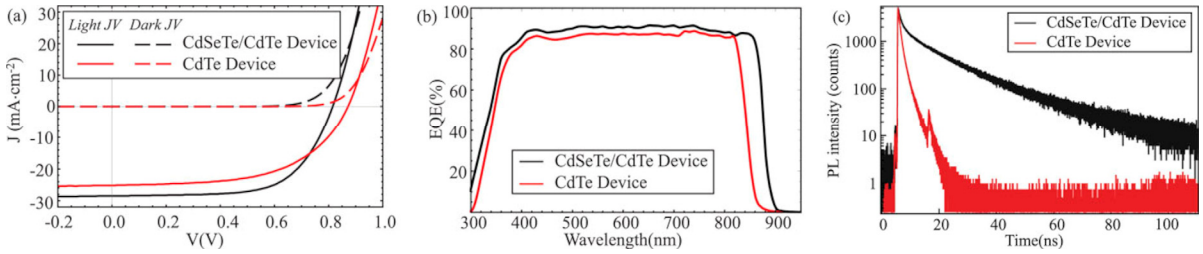

Figure 17. Performance comparison between CdSeTe/CdTe and CdTe devices. (**a**) J-V curves show higher current density for CdSeTe/CdTe, (**b**) EQE spectra indicate broader photo response for CdSeTe/CdTe, and (**c**) PL decay shows longer carrier lifetime for CdSeTe/CdTe, implying reduced recombination. Figure reproduced from [159].

Se incorporation in CdTe is typically implemented through co-evaporation or vapour transport deposition, where controlled amounts of Se are introduced at the early stages of deposition. This allows for a concentration gradient, with higher Se content at the front surface and a gradual decrease towards the back contact. This front-side Se enrichment creates a quasi-electric field that helps to separate photogenerated electron–hole pairs more efficiently, reducing recombination rates and facilitating carrier collection. This bandgap grading is also believed to enhance the carrier lifetime by minimizing recombination losses at grain boundaries, particularly where Se can diffuse and occupy Te vacancies, which are known to be major recombination centres [159].

While the incorporation of Se into CdTe significantly boosts the J_{sc} through improved infrared absorption, there is a corresponding challenge in maintaining high V_{oc}. The reduction in bandgap associated with higher Se concentrations inherently reduces the energy difference between the CB and VB, which can lead to lower V_{oc} values. To counter this, researchers are exploring graded Se profiles that optimize Se concentration near the front interface while limiting it to deeper regions to balance the trade-offs between J_{sc} and V_{oc}. Studies by Bowman et al. show that an optimal Se concentration, typically between 10 and 15% near the front, achieves the benefits of enhanced J_{sc} without excessive compromise in V_{oc}, thereby improving PCE [160].

Se incorporation in CdTe solar cells also plays a critical role in grain boundary passivation, significantly enhancing device performance. The diffusion of Se into CdTe grain boundaries reduces defect densities by passivating vacancy sites, particularly those associated with Te. This leads to a decrease in the density of deep-level traps, which are highly recombination-active and can severely limit the PCE of polycrystalline films, where grain boundaries often constitute a large fraction of the total defect population. This mechanism is supported by recent findings utilizing advanced cathodoluminescence imaging in a scanning transmission electron microscope (STEM-CL), which reveal that Se-graded CdTe, $Cd(Se_x,Te_{1-x})$, (CST) exhibits up to an order of magnitude reduction in recombination activity at grain boundaries compared to CdTe-only systems (Figure 18d) [161].

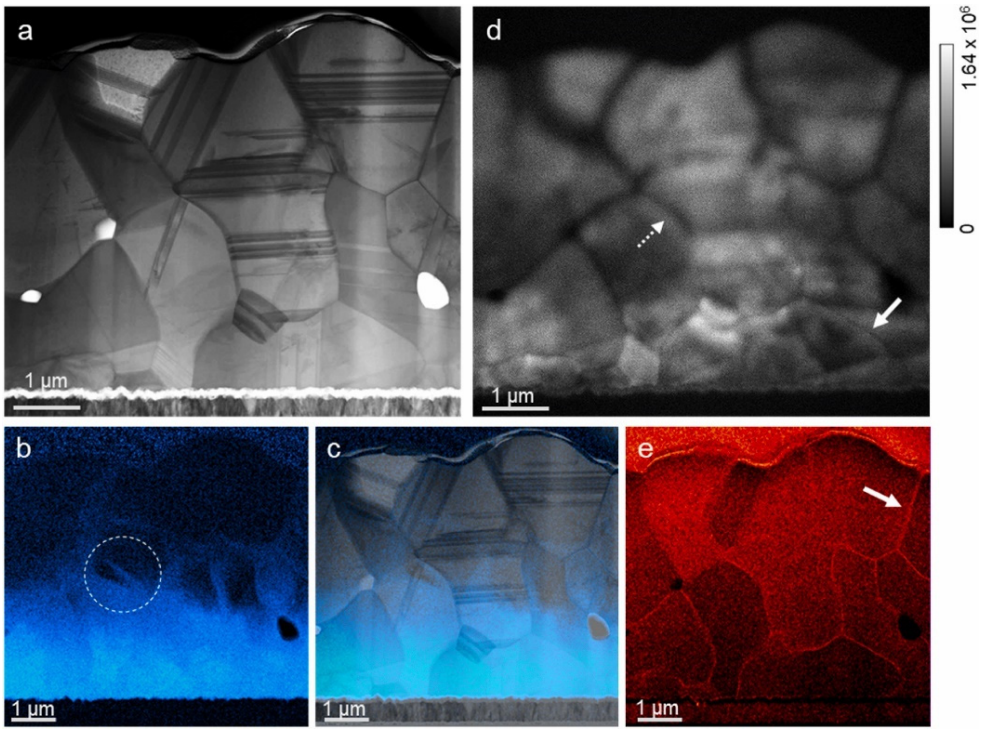

Figure 18. Cross-sectional analysis of $CdCl_2$-treated CST/CdTe bilayer solar cell. (**a**) TEM micrograph showing the structural characteristics of the bilayer, (**b**) EDX map illustrating Se distribution with notable segregation at grain boundaries. The circled region shows a boundary with an intermediated concentration of Se. (**c**) EDX map from (**b**) superimposed on (**a**). (**d**) low-temperature STEM-CL map (−170.6 °C) of panchromatic CL intensity across the cross-section, highlighting reduced grain boundary contrast in the Se-passivated CST regions compared to CdTe grain boundaries. The dashed arrow indicates thinner grain boundary contrast in the interdiffused region, while the solid arrow indicates the CST region. The intensity scale bar represents background-subtracted counts, with the background taken from the platinum region above CdTe. The reduced contrast at CST boundaries demonstrates effective Se passivation, enhancing carrier lifetime and reducing non-radiative recombination. (**e**) EDX map showing the Cl distribution. An "edge on" grain boundary in the CdTe is depicted by the arrow. Figure reproduced with permission from [161]. Licence number: 5950101435895.

DFT studies have further elucidated Se's role in reducing mid-gap states. Se appears to preferentially segregate to Te-rich grain boundaries, substituting Te atoms and mitigating mid-gap defect states, which are primarily responsible for non-radiative recombination [161]. This behaviour is consistent with studies indicating that Se incorporation leads to the elimination of deep Te–Te dangling bonds that would otherwise form defect states detrimental to carrier lifetime [22,162]. Moreover, the passivation effects achieved by Se are found to complement those from chlorine (Cl), which is introduced during the commonly used cadmium chloride ($CdCl_2$) activation treatment. Together, Se and Cl are effective in mitigating the impact of grain boundary defects that would otherwise create deep-level traps detrimental to device performance [163].

Spatially resolved PL and CL mapping of CST films indicate that Se-rich regions exhibit substantially lower non-radiative recombination rates, particularly at the grain boundaries (Figure 18b,d) [161]. However, careful control over Se distribution is necessary, as high concentrations of Se within the grain interiors can introduce sub-bandgap states, leading to below-bandgap luminescence and thus detracting from the desired radiative efficiency [161]. This suggests a nuanced trade-off in Se doping—while beneficial at grain boundaries, excessive Se in the bulk grain interiors can have adverse effects on performance, particularly by introducing new defect states.

Tong and McKenna used DFT to show that among the different types of grain boundaries in CdTe, such as the low-Σ value symmetric tilt boundaries (Σ3 (111), Σ3 (112), and Σ5 (310)), the Σ3 (111) boundary is the most stable and least detrimental to electronic properties as it does not introduce new defect states. In contrast, Σ3 (112) and Σ5 (310) grain boundaries, characterized by Te–Te and Cd–Cd dangling bonds, respectively, are prone to introducing deep-level traps [163]. Se's incorporation preferentially reduces the formation of such dangling bonds at these boundaries, thus mitigating the formation of harmful deep gap states.

Furthermore, experimental work conducted on $CdCl_2$-treated CST/CdTe bilayer devices using high-resolution TEM-CL has provided direct evidence of reduced recombination at Se-passivated grain boundaries. Specifically, the data indicate that the passivation effect induced by Se is "extra", i.e., additional to what can be achieved with Cl alone. This is clearly visualized in the Energy Dispersive X-ray Spectroscopy (EDX) maps (Figure 18), where thinner grain boundary contrasts indicate reduced recombination activity in CST compared to CdTe. This points to the synergistic effect of dual dopants in effectively reducing grain boundary recombination and enhancing carrier lifetimes, which is a critical determinant of PCE [161].

Se's role in CdTe solar cells is multifaceted. It is instrumental in passivating grain boundaries and reducing recombination losses, while also requiring precise distribution to prevent the formation of new sub-bandgap states within grain interiors. The interplay between Se's beneficial grain boundary passivation and its potential to introduce bulk defects necessitates careful optimization of doping concentrations and spatial distribution to fully leverage the advantages of CST absorber layers [160].

3.2.2. Doping

Doping strategies in CdTe solar cells are centred on improving carrier concentration, controlling defect states, and enhancing interface stability. Dopants such as Cu, Cl, and antimony (Sb) are critical for fine-tuning the electrical properties of CdTe, each with a unique impact on the carrier dynamics, recombination properties, and ultimately the performance of the solar cell.

Cu Doping: Enhancing P-Type Conductivity with Constraints

Cu is one of the most commonly used dopants in CdTe solar cells, primarily to increase p-type conductivity. Cu acts as a shallow acceptor in CdTe due to the formation of Cu_{Cd}, raising hole concentrations and improving the material's conductivity [164]. This effect can be visualized in the energy band diagram shown in Figure 19a, which illustrates the energy levels of CdTe when $Cu_{2-x}Te$ is used at the back contact. Here, the favourable alignment of energy bands facilitates p-type doping, improving the performance of the back contact.

However, Cu is highly mobile within the CdTe lattice, which can lead to issues with long-term stability and the degradation of V_{oc} over time due to Cu diffusion. The influence of Cu diffusion is also depicted in Figure 19b, where direct contact with metallic Cu is shown. The figure highlights how Cu, with its higher work function (4.77 eV), can lead to unfavourable band alignments and increased recombination if not carefully managed [164].

To mitigate these issues, advanced doping profiles limit Cu incorporation to localized regions near the back contact, where it helps form a back-surface field (BSF). This BSF is essential for reflecting minority carriers (electrons) back into the CdTe absorber, reducing recombination losses at the rear contact, as depicted in Figure 19 [165,166]. The energy barriers shown in these diagrams emphasize the importance of precise control over Cu placement to optimize the solar cell's performance.

The migration of Cu has also been observed to influence the activation of secondary phases, particularly copper telluride (Cu_2Te), at the back contact (Figure 19). This secondary phase can improve contact properties if carefully managed but may provide recombination centres if allowed to diffuse uncontrollably. Advanced passivation strategies and diffusion barriers, currently being explored to limit Cu migration, ensure it contributes positively to p-type conductivity without compromising device stability [165,167].

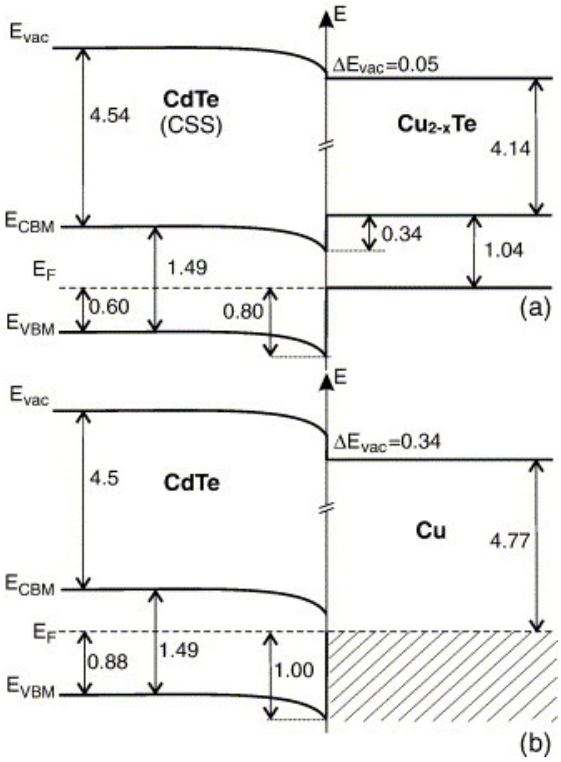

Figure 19. Energy band diagrams of CdTe with different back contact configurations. (**a**) CdTe with $Cu_{2-x}Te$ back contact, showing favourable energy alignment that supports p-type conductivity and reduces recombination. (**b**) CdTe with Cu metal contact, illustrating potential issues with energy band alignment and recombination if Cu diffusion is not carefully managed. Figure adapted with permission from [167]. Licence number: 5950110334549.

Cl Doping: Grain Boundary Passivation and Recombination Reduction

Cl treatment, often introduced through annealing with $CdCl_2$, is a well established process in CdTe solar cell fabrication for passivating grain boundaries and promoting grain growth. Cl diffuses into the CdTe lattice and preferentially localizes at grain boundaries, where it passivates defects and helps eliminate deep-level trap states [52]. This passivation significantly reduces non-radiative recombination at the boundaries, leading to longer carrier lifetimes and improved V_{oc} values [157]. Additionally, Cl treatment enhances grain growth, leading to larger grains and fewer grain boundaries, which are beneficial for carrier transport [52,157]. Dharmadasa et al. provides clear experimental evidence of these effects, showing XRD patterns (Figure 20) with improved crystallinity and increased (111) peak intensity after $CdCl_2$ treatment, which illustrates the structural enhancement due to Cl doping [157].

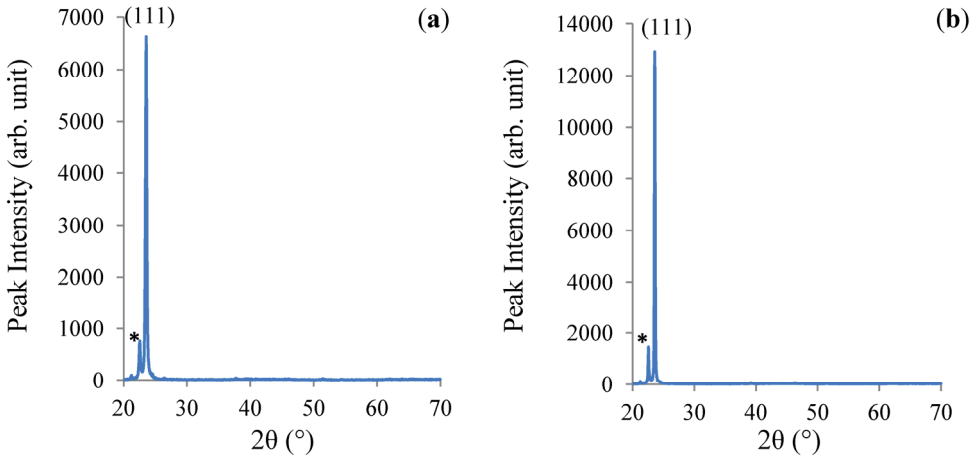

Figure 20. XRD patterns of CdTe layers before (**a**) and after (**b**) $CdCl_2$ treatment, showing increased (111) peak intensity and improved crystallinity (* represents a low-intensity peak attributed to Cd_3TeO_6, indicating surface oxidation of electroplated CdTe layers exposed to the atmosphere). Figure reproduced from [157].

The introduction of Cl during $CdCl_2$ annealing effectively mitigates the detrimental effects of dangling bonds, such as Te–Te bonds, which commonly occur at certain grain boundaries in CdTe, like the Σ3 (112) and Σ5 (310) boundaries. Studies have highlighted that Cl, often co-doped with Na, can passivate these gap states induced by dangling bonds, significantly enhancing material quality and reducing recombination losses at grain boundaries [163]. Recent studies have also focused on optimizing Cl concentrations to achieve maximum passivation without introducing new defect states, as excess Cl can lead to the formation of Cl-rich phases, which may degrade device performance [52,157].

TEM images (Figure 21) by Dharmadasa et al. further support this discussion as they clearly show the increase in grain size and the reduction in grain boundary density after $CdCl_2$ treatment [157]. The formation of large grains, extending from the CdS layer to the top surface, is a key property needed for high PCE solar cells, reinforcing the role of Cl treatment in enhancing grain structure.

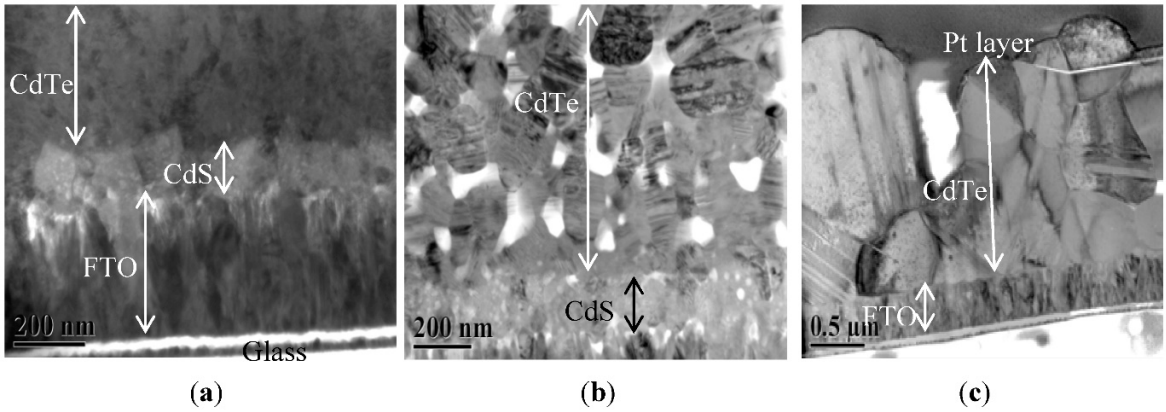

Figure 21. TEM images illustrating the effects of $CdCl_2$ treatment. (**a**) As-deposited glass/FTO/CdS/CdTe, (**b**) heat-treated with 0.01% $CdCl_2$, and (**c**) heat-treated with 1.0% $CdCl_2$. The treatment results in larger grains, reduced grain boundary density, and complete absorption of the CdS layer into the CdTe layer, with grain sizes comparable to the CdTe layer thickness. Figure reproduced from [157].

These combined Cl and Se treatments allowed CdTe solar cells to reach a PCE of over 22%, with optimized V_{oc} values due to improved bulk passivation, larger grain sizes, and

reduced recombination losses at grain boundaries [52]. The interplay between Cl and Se, as well as innovations in CdTe microstructure control, remain crucial for advancing CdTe solar technology towards the next milestones in device performance.

Group V Dopants: Arsenic, Phosphorus, and Sb Doping in CdTe

Arsenic (As), phosphorus (P), and antimony (Sb) are effective group-V p-type dopants for CdTe, each contributing distinct benefits to enhancing hole concentration, conductivity, and V_{oc}, which collectively improve the PCE of CdTe solar cells. These dopants stabilize p-type properties and boost overall cell performance, although their stability, toxicity, and compatibility with processing conditions vary.

As, P, and Sb substitute for Te in the CdTe lattice, creating shallow acceptor states that improve p-type conductivity, particularly when doping occurs under Cd-rich conditions, which reduces the formation of compensating defects [158]. As has been found to enhance bulk recombination properties by reducing deep-level defects, leading to longer carrier lifetimes and improved V_{oc}. Compared to Cu, As has lower mobility, providing enhanced long-term stability [158]. P similarly substitutes for Te, resulting in stable p-type conductivity and improved hole density. It is particularly beneficial in polycrystalline films, reducing grain boundary recombination and enhancing V_{oc} due to improved carrier lifetimes. Additionally, P-doped CdTe is compatible with high-temperature processing, making it suitable for scalable manufacturing [158]. Sb enhances band alignment at interfaces, especially with the back contact, facilitating efficient hole transport and minimizing recombination losses. It also modifies grain boundary properties, minimizing recombination and supporting the effects of Cu and Cl in complex device structures [55,168,169].

Figure 22 shows the correlation between Group-V dopant concentration and hole concentration for As, P, and Sb, demonstrating their ability to achieve high p-type conductivity. The data reveal that both bulk and film samples of these dopants display a strong correlation between atomic concentration and hole concentration, with Sb performing comparably to As and P, especially at elevated dopant levels.

Although effective, each dopant has its challenges. As is prone to forming AX centres—defect complexes that trap holes, reducing carrier concentration. To mitigate this, rapid thermal quenching is used to maintain As in its acceptor state, minimizing defect formation [158]. Techniques such as molecular beam epitaxy (MBE) also allow precise control over As incorporation, reducing the likelihood of self-compensation. P, on the other hand, can form recombination-inducing defect complexes with Cd vacancies. To overcome this, doping under Cd-rich conditions is employed, complemented by rapid thermal processing to enhance P activation, which increases hole density and reduces recombination at interfaces [158]. Sb forms deeper acceptor states than Cu, yielding stable p-type conductivity with reduced migration and improved long-term stability [55,156,158].

Toxicity and environmental impact are also important considerations. As is highly toxic, requiring careful handling during manufacturing and disposal. P is a less toxic alternative, making it more environmentally friendly. Sb, besides being less toxic than As, also provides significant improvements in stability and carrier transport, positioning it as a promising dopant for scalable solar cell production [55,156,158].

Overall, while As, P, and Sb each serve as effective p-type dopants for CdTe, they offer different advantages. As provides superior stability and reduced deep-level defects but carries toxicity concerns. P is safer and compatible with high-temperature processing, but requires careful control to avoid self-compensation. Sb provides stable p-type properties, enhances band alignment, and improves grain boundary characteristics, making it a strong candidate for long-term applications and a useful complement to other dopants. The

choice between these dopants depends on the desired balance between device performance, stability, and environmental impact.

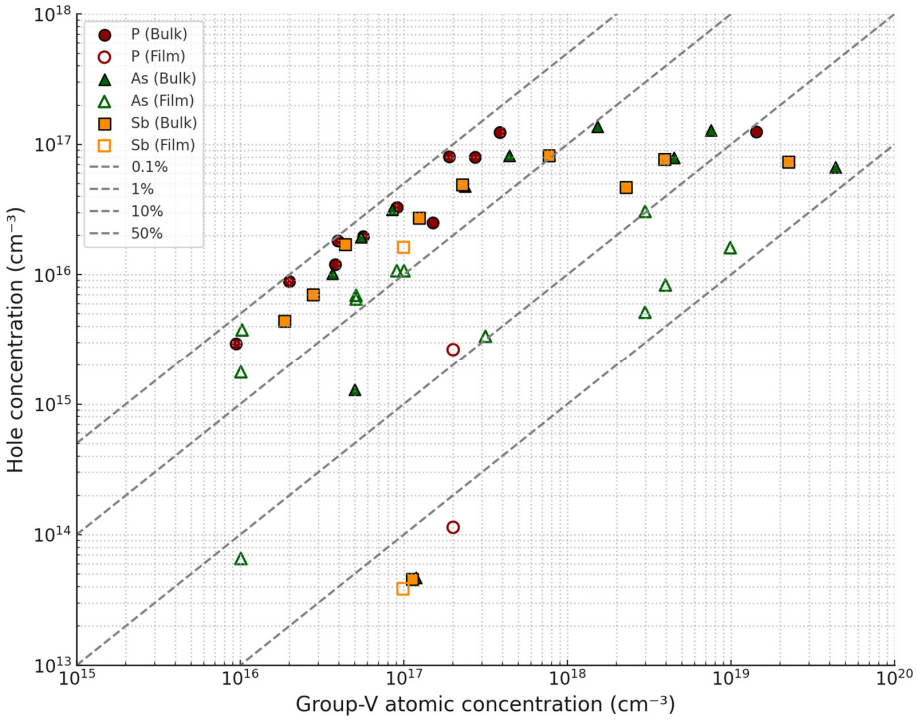

Figure 22. Hole concentration as a function of Group-V atomic concentration for different dopants (P, As, Sb) in CdTe. Data points for bulk and film samples indicate doping efficiency and demonstrate the effectiveness of P, As, and Sb in achieving high p-type conductivity. Reconstructed image based on data from [158].

Interplay of Multiple Dopants in Advanced CdTe Devices

The combined effects of Cu, Cl, and Sb dopants in CdTe solar cells reveal a complex interplay that affects multiple aspects of device performance. While Cu enhances conductivity, Cl promotes passivation, and group V elements provides stability, their interactions must be carefully managed to avoid unwanted phase formation or degradation. For example, excessive Cu in the presence of Cl can lead to the formation of CuCl clusters, which introduce deep traps and negatively impact carrier lifetimes. Similarly, high concentrations of Sb can alter the doping profile, potentially shifting the Fermi level and impacting the p-n junction properties.

Advanced doping profiles that use spatial control over each dopant's incorporation are now being developed to achieve a balanced, synergistic effect. Techniques such as atomic layer deposition (ALD) and MBE allow for atomic-level precision in doping, enabling researchers to tailor the dopant distribution within the CdTe layer for optimized band alignment, reduced recombination, and improved stability [159,160].

3.2.3. Interface and Buffer Layer Optimization

Using Buffer Layers for Junction Optimization

Interface engineering has been a pivotal area of research to address the recombination and band alignment challenges at the CdTe/CdS junction. The inclusion of buffer layers like magnesium zinc oxide (MgZnO) has been shown to be beneficial in tailoring the band structure at the CdTe/CdS interface, enhancing both V_{oc} and J_{sc}.

MgZnO, with its high bandgap, serves as an effective buffer layer that improves the electron affinity mismatch between CdTe and typical TCO layers. This alignment reduces the energy barrier for electron transport, enhancing charge collection and reducing interface recombination. By adjusting the Mg content in MgZnO, researchers can fine-tune

the CB position to better align with CdTe, thereby optimizing the overall PCE of the solar cell. MgZnO also exhibits better stability compared to traditional CdS layers, making it a promising choice for enhancing long-term device performance [160].

In cases where CdS alone is employed, the thickness and stoichiometry of the CdS layer are critical factors. A thinner CdS layer increases light transmission to the CdTe absorber, improving the J_{sc}, but can also increase the likelihood of pinholes, leading to shunting issues. Advances in ALD, CBD and other deposition techniques have allowed for better control over CdS thickness and composition, resulting in improved device performance without sacrificing stability [55].

Impact of Passivation and Carrier Transport on Efficiency

The role of passivation in CdTe solar cells is paramount, as it directly affects the carrier lifetime and reduces defect-assisted recombination, thereby influencing V_{oc} and FF. Passivation techniques primarily involve the use of Cl and other halides, which diffuse into grain boundaries during PDT. This treatment passivates surface states and fills defect levels, allowing for more effective carrier transport and reduced recombination at critical interfaces.

Carrier transport at the CdTe/CdS junction is sensitive to interface quality, which can be significantly enhanced through passivation. The introduction of controlled passivation layers, such as MgZnO, along with halide treatments, has allowed CdTe cells to achieve higher V_{oc} and FF by reducing recombination at both grain boundaries and interfaces. This strategy has enabled CdTe solar cells to reach PCE at approaching the 22% mark [22,53].

Moreover, advanced passivation techniques have helped in stabilizing CdTe devices under various operational conditions. By improving the quality of interfaces through both chemical and physical passivation, CdTe solar cells can achieve enhanced performance consistency and longevity. Research continues to focus on refining these techniques, with recent studies exploring the use of novel materials for passivation layers, aiming to achieve further reductions in recombination and improved carrier transport across all interfaces [165].

3.3. CZTS/CZTSSe

3.3.1. Bandgap Engineering

Bandgap engineering in CZTS/CZTSSe solar cells aims to address the inherent limitations in PCE and stability by optimizing key parameters such as sulfurization conditions, doping strategies, and interface engineering. These approaches enhance the light absorption, reduce defect densities, and improve the PV properties of CZTS/CZTSSe-based devices. The following sections detail recent advances in each of these areas, highlighting their contributions to achieving higher PCE and mitigating common performance bottlenecks.

Sulfurization and S/Se Ratio Optimization

Sulfurization is a critical process in CZTSSe fabrication, enabling precise control over the composition and bandgap of the absorber layer by modulating the S/Se ratio. The choice between S-rich and Se-rich configurations has profound implications for the optical and electronic properties of the CZTSSe layer. In recent studies, S-rich CZTS (so termed when S content is dominant) has been favoured for applications targeting the visible spectrum, owing to its bandgap of around 1.5 eV, which aligns with peak solar irradiance [77,170]. Conversely, Se-rich CZTSSe (termed CZTSe when Se content is dominant) presents a lower bandgap near 1.0 eV, which enhances absorption in the near-infrared region and is beneficial in tandem cell configurations.

Recent work has focused on optimizing sulfurization parameters, including temperature, time, and gas flow, to stabilize the CZTS phase and prevent the formation of secondary phases like Cu_2S and SnS_2, which adversely affect PCE [72,80]. Studies have shown that the presence of H_2S gas in the sulfurization atmosphere can significantly impact film morphol-

ogy, grain size, and composition. For example, Hajara et al. demonstrated that controlling the H_2S flow rate during the sulfurization process can tune the bandgap of CZTS films from 1.28 to 1.74 eV, with high S flow rates reducing the Zn/Sn ratio and introducing S-rich surface aggregates that affect the electrical characteristics [80].

Furthermore, the S/Se ratio has been extensively studied in mixed-phase CZTSSe materials, where intermediate compositions are formed by partially replacing S with Se. This approach enables fine bandgap modulation, balancing the benefits of both elements. Se incorporation during high-temperature annealing has been shown to enhance the crystallinity and grain size of CZTSSe, reducing boundary recombination and improving charge carrier mobility [76,77]. Jiang et al. highlighted that the Se content could be tailored by introducing Se vapour during annealing, effectively reducing the optical bandgap and producing more compact and crystalline CZTSSe films [77]. This enhanced structural quality has resulted in devices with improved J_{sc} due to increased light absorption and reduced recombination losses, thus pushing device performance closer to theoretical limits.

Challenges in Bandgap Engineering for CZTSSe

Despite these advances, challenges remain in achieving consistent control over defect formation during bandgap tuning in CZTSSe. The complex chemistry of CZTSSe compounds inherently leads to a high density of intrinsic defects and secondary phases, which complicates the process of defect mitigation and control. Recent studies have highlighted the importance of defect passivation techniques, such as MAPDA and PDT, to reduce deep-level defects and suppress defect clusters like [CuZn + SnZn], which are major contributors to band tailing and recombination losses [73,79]. These innovations have shown potential in stabilizing the bandgap and enhancing device performance, but further research is needed to refine these techniques for industrial scalability. Thus, while advances in sulfurization, doping, and interface engineering have contributed significantly to the progress of CZTS/CZTSSe-based solar cells, precise control over defect formation and passivation remains a critical challenge in realizing the full efficiency potential of CZTS/CZTSSe materials.

3.3.2. Doping Strategies

Doping CZTS/CZTSSe with elements such as Germanium (Ge), Ag, Na, and Cobalt (Co) has proven effective in reducing defect density, passivating surface states, and optimizing the material's optoelectronic properties. Recent advances in this area have introduced innovative doping methods to address specific defects that contribute to V_{oc} deficits and charge carrier recombination.

Ag Doping

Ag doping in CZTS is an effective strategy to enhance PCE by reducing defect concentration, improving crystallinity, and altering optical properties. Ag incorporation substitutes Cu in the kesterite lattice, reducing Cu_{Zn} antisite defects, which create recombination centres that hinder performance.

Nguyen et al. showed that Ag incorporation up to a Ag/(Ag + Cu) ratio of 0.02 improved grain size and morphology and reduced pinholes in CZTS films, enhancing PCE due to better band alignment at the CdS/CZTS interface and fewer Cu_{Zn} defects [171]. The SEM image (Figure 23) of the CZTS films after Ag incorporation illustrates the improvement in grain size and reduced pinholes. Gour et al. also found that Ag doping improved structural quality, resulting in a rice-like morphology, increased grain size, and higher optical absorption. Ag's monovalent state helps stabilize the structure and reduce secondary phase formation compared to Cu [172].

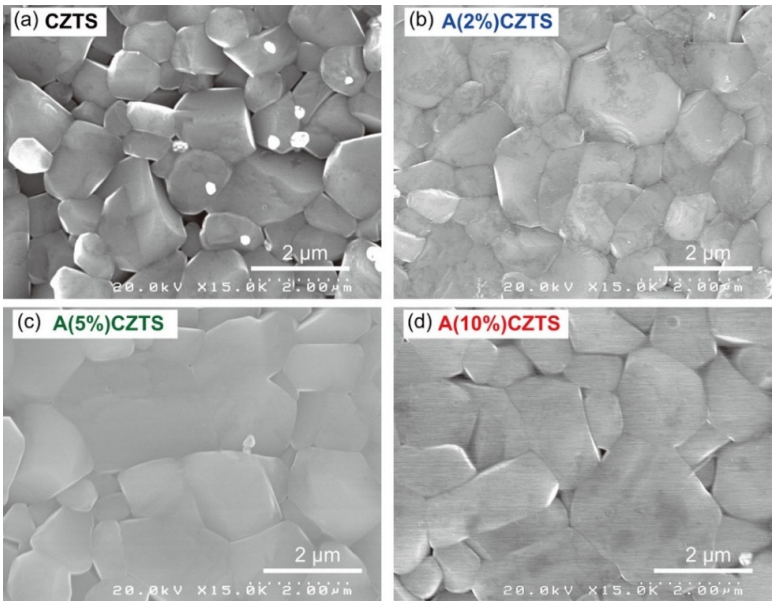

Figure 23. SEM images of (**a**) undoped CZTS, (**b**) A(2%)CZTS, (**c**) A(5%)CZTS, and (**d**) A(10%)CZTS thin films, showing the enhanced grain size and void reduction in Ag-incorporated CZTS compared to undoped CZTS. Reprinted with permission from [171]. Copyright (2024) American Chemical Society.

Saha et al. observed that Ag-doped CZTSSe films exhibited reduced V_{oc} deficits and improved FF, attributed to Ag's role in modifying the grain boundary passivation and increasing the built-in electric field across the absorber layer [173]. Atasoy et al. and Nazari and Dhakal highlighted the role of Ag in enhancing grain quality and reducing defects in Ag-doped CZTSe (ACZTSe) and CZTS cells. Ag contributed to significant grain growth and reduced defect concentrations, increasing PCE from 5% to over 8%. In CZTS, Ag-doping improved grain size and electrical properties, reducing series resistance and increasing shunt resistance, which improved the PCE from 5.84% to 6.66% [174,175].

Ibrahim et al. introduced a double-layer solution-processed CZTS solar cell doped with Ag and K. Combining Ag and K in a double-layer absorber structure (ACZTS-KCZTS) reduced the V_{oc} deficit and increased J_{sc}, leading to better carrier collection and fewer voids, resulting in an optimized PCE of 8.24% [176]. Figure 24 shows the J-V characteristics and EQE of the ACZTS-KCZTS device, illustrating the improved electrical performance due to the incorporation of Ag and K.

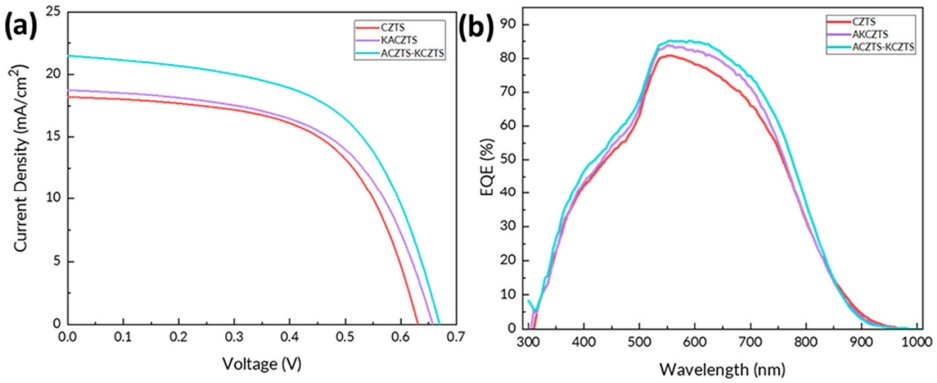

Figure 24. (**a**) J-V characteristics of CZTS, single-layer Ag-alloyed and K-doped CZTS (KACZTS), and ACZTS-KCZTS solar cells, illustrating the current density versus voltage behaviour. (**b**) EQE curves for CZTS, KACZTS, and ACZTS-KCZTS devices, showing PCE across different wavelengths. ACZTS-KCZTS exhibits enhanced performance in both current density and EQE compared to other compositions. Reprinted with permission from [176]. Copyright (2024) American Chemical Society.

Ge Doping

Ge doping in CZTS and CZTSSe has been extensively investigated to enhance the performance of these kesterite-based solar cells. Ge incorporation has been shown to significantly improve the crystallinity, reduce defect concentration, and enhance the V_{OC}, leading to higher conversion efficiency.

The primary advantage of Ge doping lies in mitigating Sn-related defects, particularly Sn_{Zn} antisite defects, which introduce mid-bandgap states that facilitate charge carrier recombination. Studies have demonstrated that Ge incorporation leads to the suppression of these defects, resulting in an improved electronic landscape and enhanced V_{OC}. Naylor et al. reported that Ge doping during the selenization process improves crystallinity, grain morphology, and overall efficiency in CZTSSe solar cells. By doping with Ge, they observed that the average crystallite size increased from 40 nm to 88 nm, and the lateral grain sizes exceeded 1 μm in thickness. The improved structural and electronic properties enabled a V_{oc} increase of up to 25 mV and a PCE improvement of more than 1%, with a maximum of 6.45% in their samples. These enhancements were attributed to the Ge–Se growth mechanism, which facilitated recrystallization and reduced Sn-related disorder at the CZTSSe/CdS interface [177].

Li et al. demonstrated that Ge doping promotes grain growth, resulting in a compact film morphology with fewer pinholes and increased surface roughness, which rose from 75 nm in undoped films to 96 nm in films doped with Ge. This effect is attributed to Ge preferentially interacting with Se during selenization, forming GeSe and $GeSe_2$ phases that enhance crystallization. The formation of tensile stress, caused by lattice shrinkage due to Ge's smaller atomic radius compared to Sn, further suppresses secondary phase formation. The study also reported a significant improvement in device performance, with a Ge-doped CZTSSe solar cell achieving a PCE of 5.38%, an increase of 25.4% compared to undoped cells, which had a PCE of 4.29%, alongside a V_{oc} of 403 mV and a J_{sc} of 28.51 mA/cm^2. Ge doping also resulted in better charge carrier collection by reducing bulk recombination and improving the CZTSSe/CdS interface properties [178].

Further studies by Atasoy et al. revealed that co-doping CZTSe with Ag and Ge significantly improves the crystalline quality, reduces defect concentration, and leads to larger grain sizes, thereby enhancing overall solar cell efficiency. The synergistic effect of Ag and Ge during high-temperature annealing at 550 °C effectively suppresses defect formation and enhances crystallization. Notably, the incorporation of 10% Ag and 7% Ge into CZTSe resulted in a PCE of 8.46%, compared to 7.53% for samples with 10% Ag alone and 5.20% for samples with 7% Ag. This improvement is attributed to the formation of a Ge-back gradient, which acts as a BSF, and an Ag-front gradient, which mitigates recombination losses near the p-n junction. Additionally, the optical bandgap was observed to increase to approximately 1.10 eV, contributing to improved device performance [174,179].

Overall, Ge doping in CZTS and CZTSSe effectively enhances device performance by improving crystallinity, reducing defect concentrations, and promoting grain growth. In CZTSSe, the presence of Se further amplifies these effects, resulting in greater efficiency gains compared to CZTS.

Co Doping

Co doping is a more recent approach that introduces magnetic properties to CZTS while modifying the optoelectronic characteristics. Co-doped CZTS has shown promise in enhancing light absorption (Figure 25) due to its magnetic interactions, which may influence the electronic structure of CZTS, although this area remains in the early research stages [180]. Co doping also appears to increase grain size, similar to Ag, contributing to reduced recombination at grain boundaries and enhanced carrier lifetimes.

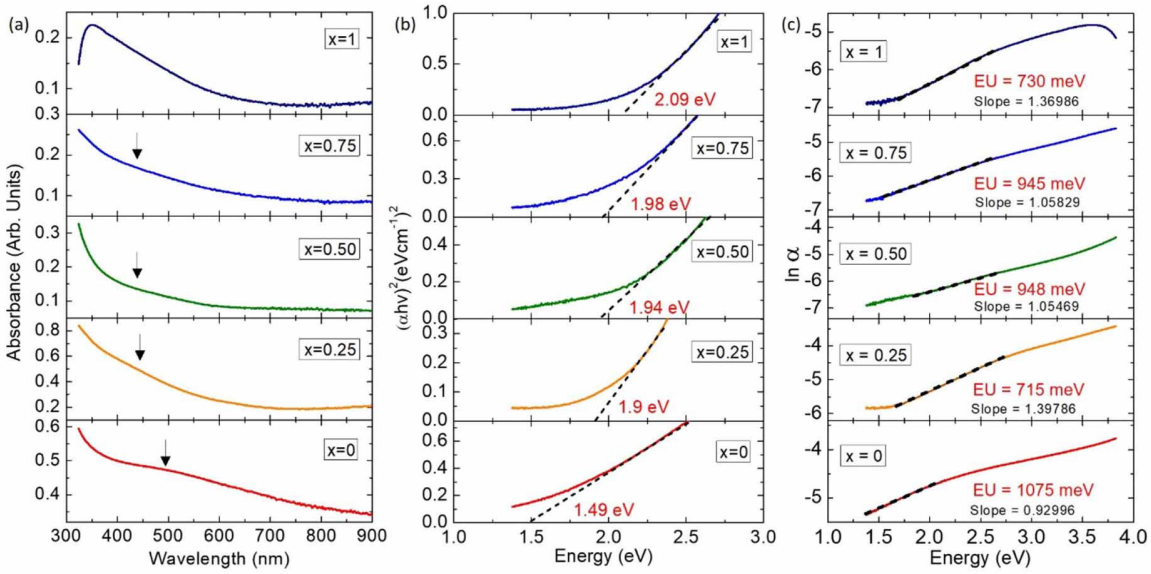

Figure 25. (**a**) Absorbance spectra of samples with varying Co amounts (x), showing a shift in the absorption edge as the composition changes. (**b**) Tauc plot analysis to estimate the optical bandgap energies for each sample, highlighting a decrease in bandgap energy as the amount of Co increases. (**c**) Urbach energy analysis using the logarithm of the absorption coefficient, indicating variations in Urbach energy and slopes for different compositions, illustrating the influence of disorder in the materials as x varies. Figure reproduced with permission from [180]. Licence ID: 1567181-1.

Alkali Metal Doping

Alkali metals such as Na and K have shown substantial benefits in improving carrier concentrations and mobilities in CZTS/CZTSSe. Na doping, specifically, has been effective in increasing grain size and improving crystal quality, often resulting in enhanced J_{sc} and V_{oc}. Nugroho et al. demonstrated that Na-doped CZTS films prepared via non-vacuum processes had fewer surface defects, lower resistivity, and more stable photoactive phases [75]. Na-PDT have also been shown to aid in shallow defect passivation, which is crucial for reducing non-radiative recombination and increasing V_{oc}.

3.3.3. Buffer Layer Advancements and Interface Engineering

One of the significant advances in recent CZTS/CZTSSe research has been in interface engineering to reduce recombination losses at the p-n junction interface. Bandgap engineering at the HJT interfaces has been essential for minimizing interface recombination, which is a critical factor limiting V_{oc} in CZTS/CZTSSe devices.

Buffer Layer Innovations

Traditional CdS buffer layers, while effective, present environmental and cost concerns due to Cd's toxicity. Novel buffer materials have been explored as potential replacements for CdS. WO_3 has shown promising results, offering a wider bandgap that better aligns with CZTS, resulting in improved V_{oc} and reduced band tailing effects at the interface. Furthermore, WO_3 buffer layers, when combined with CZTSe BSF layers, have demonstrated significant PCE gains by enhancing carrier collection and reducing rear-side recombination losses [181]. Meanwhile, materials like WS_2, ZrS_2, MoS_2, and transitional metal oxynitrides have been evaluated through numerical simulations, revealing their potential benefits for CZTS solar cells.

For instance, the study by Riyad et al. introduces WS_2 as a buffer layer for CZTS solar cells to replace CdS. Simulations showed that WS_2 forms a spike-like band structure at the CZTS/WS_2 interface, which reduces non-radiative recombination losses, contributing to

improved device efficiency. They reported a significant simulated PCE of 30.63% under optimized conditions. Additionally, Sb_2S_3 was used as a hole transport layer (HTL) in the simulations to further enhance efficiency by minimizing back surface recombination [182].

Moustafa et al. explored the use of ZrS_2 as a novel, nontoxic buffer layer for CZTS-based solar cells. Their numerical simulations indicated that ZrS_2 provides favourable band alignment at the interface with CZTS, yielding a PCE of approximately 17.61%. The ZrS_2 layer also benefits from being earth-abundant and environmentally friendly, which makes it a promising replacement for CdS [183].

Another approach explored by Ghosh et al. involves using MoS_2 as a buffer layer in conjunction with graphene as a TCO layer. Simulations demonstrated that MoS_2 offers a suitable bandgap and high carrier mobility, which leads to enhanced quantum efficiency and a simulated PCE of 18.27%. This combination aims to improve both the electrical and optical properties of the solar cell, and the use of graphene further enhances transparency and stability [184].

Chen et al. investigated the potential of transitional metal oxynitrides, specifically TiN_xO_y and CrN_xO_y, as buffer layers in CZTS solar cells. Simulations revealed that both materials could improve efficiency, with TiN_xO_y showing better band offset compatibility compared to CrN_xO_y. This optimization resulted in a simulated PCE of around 22%, which makes TiN_xO_y a compelling candidate for buffer layer replacement in CZTS devices [185].

Defect Passivation at the Interface

Recent innovations include passivation treatments such as moisture-assisted post-deposition annealing (MAPDA), which reduce the concentration of Na and mitigate deep-level defects in the CZTS absorber. Sun et al. reported that MAPDA in a moist N_2 environment allowed for Na extraction from the CZTS bulk and the diffusion of favourable Cd atoms into the CZTS grain boundaries during CBD of the CdS layer. This effectively suppresses deep-level recombination centres, such as the [Cu_{Zn} + Sn_{Zn}] defect cluster, thereby enhancing V_{oc} and minimizing interface-related losses [79].

Interface Layering

Studies demonstrate that tailoring the bandgap of interface layers can create a “graded” bandgap structure that facilitates smoother energy transitions and reduces potential barriers for carrier transport. For instance, incorporating multi-layered configurations, such as CZTSe as a BSF in CZTS cells (WO_3/CZTS/CZTSe), improves charge separation and reduces recombination at interfaces. This is achieved through optimized conduction band alignment, minimizing defects and recombination losses. Interface grading is particularly valuable in tandem solar cells, where precise bandgap engineering enables the effective integration of low-bandgap CZTSe with high-bandgap top cells, thereby enhancing power conversion efficiency (PCE) [71,181].

These combined strategies in bandgap engineering—through sulfurization optimization, selective doping, and advanced interface engineering—represent substantial progress in addressing the inherent challenges of CZTSSe solar cells. By reducing recombination losses, improving charge transport, and stabilizing the bandgap properties, these techniques bring CZTSSe technology closer to achieving PCE results that are competitive with other thin-film solar cell technologies, such as CIGS and CdTe. The implementation of these techniques, however, requires precise process control and optimization to ensure scalability and reproducibility for industrial applications.

4. Conclusions

The advancements in TFSC, particularly in materials like CIGS, CdTe, and CZTSSe, have undergone considerable improvements in PCE through targeted innovations such as bandgap engineering, alkali metal doping, and interface optimization. Specifically, the adaptability of CIGS through Ga and Ag alloying, the successful Se incorporation in CdTe for enhanced light absorption, and S/Se ratio optimization in CZTSSe have collectively addressed key performance barriers. Each material exhibits unique advantages that contribute to their versatility in applications ranging from BIPV to portable devices. However, challenges related to stability and scalability remain, motivating ongoing research to further enhance performance and environmental sustainability. Overall, the continued development of these technologies is crucial for TFSCs to reach their full potential in contributing to the global transition towards renewable energy.

Funding: This research was funded by FEDER funds through the COMPETE 2020 Program and National Funds through FCT—Portuguese Foundation for Science and Technology under the projects LISBOA-01-0247-FEDER-039985/POCI-01-0247-FEDER-039985, LA/P/0037/2020, UIDP/50025/2020, and UIDB/50025/2020 of the Associate Laboratory Institute of Nanostructures, Nanomodelling and Nanofabrication—i3N.

Conflicts of Interest: The authors declare no conflicts of interest.

References

1. Oni, A.M.; Mohsin, A.S.M.; Rahman, M.M.; Bhuian, M.B.H. A Comprehensive Evaluation of Solar Cell Technologies, Associated Loss Mechanisms, and Efficiency Enhancement Strategies for Photovoltaic Cells. *Energy Rep.* **2024**, *11*, 3345–3366.
2. Namnuan, B.; Chatraphorn, S. Improving the Photovoltaic Performance of CIGS Solar Cells with the Modified 3-Stage Co-Evaporation Process. *Mater. Sci. Semicond. Process.* **2024**, *179*, 108485.
3. Karami, A.; Morawski, M.; Kempa, H.; Scheer, R.; Cojocaru-Miredin, O. Sodium in Cu(In,Ga)Se_2 Solar Cells: To Be or Not to Be Beneficial. *Solar RRL* **2024**, *8*, 2300544.
4. Libório, M.S.; Queiroz, J.C.A.d.; Sivasankar, S.M.; Costa, T.H.d.C.; Cunha, A.F.d.; Amorim, C.d.O. A Review of Cu_3BiS_3 Thin Films: A Sustainable and Cost-Effective Photovoltaic Material. *Crystals* **2024**, *14*, 524. [CrossRef]
5. Amorim, C.O.; Liborio, M.S.; Queiroz, J.C.A.; Melo, B.M.G.; Sivasankar, S.M.; Costa, T.H.C.; Graça, M.P.F.; da Cunha, A.F. Cu_3BiS_3 Film Synthesis through Rapid Thermal Processing Sulfurization of Electron Beam Evaporated Precursors. *Emergent Mater.* **2024**, 1–13. [CrossRef]
6. Santana Liborio, M.; Amorim, C.O.; Queiroz, J.C.A.; Sivasankar, S.M.; Costa, T.H.d.C.; da Cunha, A.F. Strategies to Enhance the Efficiency of Cu_3BiS_3-Based Photovoltaic Devices: Simulation Insights and Buffer Layer Engineering. *ACS Appl. Opt. Mater.* **2024**, *3*, 81–90. [CrossRef]
7. Kawano, Y.; Chantana, J.; Nishimura, T.; Mavlonov, A.; Minemoto, T. [Ga]/([Ga]+[In]) Profile Controlled through Ga Flux for Performance Improvement of Cu(In,Ga)Se_2 Solar Cells on Flexible Stainless Steel Substrates. *J. Alloys Compd.* **2022**, *899*, 163276. [CrossRef]
8. Bremaud, D.; Rudmann, D.; Bilger, G.; Zogg, H.; Tiwari, A.N. Towards the Development of Flexible CIGS Solar Cells on Polymer Films with Efficiency Exceeding 15%. In Proceedings of the Conference Record of the Thirty-First IEEE Photovoltaic Specialists Conference, 2005, Lake Buena Vista, FL, USA, 3–7 January 2005; IEEE: New York, NY, USA, 2005; pp. 223–226.
9. Chirilă, A.; Buecheler, S.; Pianezzi, F.; Bloesch, P.; Gretener, C.; Uhl, A.R.; Fella, C.; Kranz, L.; Perrenoud, J.; Seyrling, S.; et al. Highly Efficient Cu(In,Ga)Se_2 Solar Cells Grown on Flexible Polymer Films. *Nat. Mater.* **2011**, *10*, 857–861. [CrossRef]
10. Khatri, I.; LaGrow, A.P.; Bondarchuk, O.; Nicoara, N.; Sadewasser, S. Effect of Solution-Processed Cesium Carbonate on Cu(In,Ga)Se_2 Thin-Film Solar Cells. *Prog. Photovolt.* **2024**, *32*, 864–871.
11. Yu, H.; Choi, E.P.; Chai, S.U.; Lee, S.H.; Park, H.K.; Kim, G.Y.; Jo, W.; Kim, W.M.; Kim, D.; Joo, B.; et al. Anisotropic Charge Transport in Cu(In,Ga)Se_2 by Heavy Alkali Postdeposition Treatment for Reducing Cell-to-Module Efficiency Loss in Monolithically Integrated Photovoltaic Modules. *Solar RRL* **2023**, *7*, 2300055. [CrossRef]
12. Pinarbasi, M.; Aksu, S.; Freitag, J.; Boone, T.; Zolla, H.; Vasquez, J.; Nayak, D.; Lee, E.; Wang, T.; Abushama, J.; et al. Roll to Roll Manufacturing of Flexible CIGS Cells and Panels. In Proceedings of the 25th European Photovoltaic Solar Energy Conference and Exhibition/5th World Conference on Photovoltaic Energy Conversion, Valencia, Spain, 6–10 September 2010.
13. Li, J.; Sun, K.; Yuan, X.; Huang, J.; Green, M.A.; Hao, X. Emergence of Flexible Kesterite Solar Cells: Progress and Perspectives. *Npj Flex. Electron.* **2023**, *7*, 16. [CrossRef]

14. Ramanujam, J.; Singh, U.P. Copper Indium Gallium Selenide Based Solar Cells—A Review. *Energy Environ. Sci.* **2017**, *10*, 1306–1319. [CrossRef]
15. Shao, X.; Shi, S.; Liang, B.; Chen, L.; Qi, T.; Yuan, X.; Yu, S.; Tang, W.; Yang, C.; Li, W. Alkali Metal Pretreatment for Precise Na Doping and V_{oc} Improvement in CIGS Thin-Film Solar Cells. *ACS Appl. Mater. Interfaces* **2024**, *16*, 30147–30156. [CrossRef]
16. Miller, M.F.; Kanevce, A.; Bothwell, A.M.; Paetel, S.; Kuciauskas, D.; Arehart, A.R. Defects in RbF-Treated Cu(In_xGa_{1-x})Se_2 Solar Cells and Their Impact on V_{oc}. In Proceedings of the 2023 IEEE 50th Photovoltaic Specialists Conference (PVSC), San Juan, PR, USA, 11–16 June 2023.
17. Hill, T.; Grover, S.; Sites, J. Widegap CdSe Solar Cells with V_{oc} > 750 mV. In Proceedings of the 2023 IEEE 50th Photovoltaic Specialists Conference (PVSC), San Juan, PR, USA, 11–16 June 2023; pp. 1–6.
18. Elanzeery, H.; Stlzel, M.; Eraerds, P.; Borowski, P.; Aboulfadl, H.; Lomuscio, A.; Helmecke, D.; Schubbert, C.; Oueslati, S.; Hla, M.; et al. Beyond 20% World Record Efficiency for Thin-Film Solar Modules. *IEEE J. Photovolt.* **2023**, *14*, 107–115. [CrossRef]
19. Mwenda, P.M.; Njoroge, W.; Mirenga, S.; Kinyua, D.M. Review: Advances in the CIGS Thin Films for Photovoltaic Applications. *Smart Grid Renew. Energy* **2022**, *13*, 75–87. [CrossRef]
20. Afre, R.A.; Pugliese, D. Perovskite Solar Cells: A Review of the Latest Advances in Materials, Fabrication Techniques, and Stability Enhancement Strategies. *Micromachines* **2024**, *15*, 192. [CrossRef] [PubMed]
21. Green, M.A.; Dunlop, E.D.; Yoshita, M.; Kopidakis, N.; Bothe, K.; Siefer, G.; Hao, X. Solar Cell Efficiency Tables (Version 63). *Prog. Photovolt. Res. Appl.* **2024**, *32*, 3–13. [CrossRef]
22. Sharma, I.; Pawar, P.S.; Kumar Yadav, R.; Nandi, R.; Heo, J. Review on Bandgap Engineering in Metal-Chalcogenide Absorber Layer via Grading: A Trend in Thin-Film Solar Cells. *Sol. Energy* **2022**, *246*, 152–180. [CrossRef]
23. Keller, J.; Kiselman, K.; Donzel-Gargand, O.; Martin, N.M.; Babucci, M.; Lundberg, O.; Wallin, E.; Stolt, L.; Edoff, M. High-Concentration Silver Alloying and Steep Back-Contact Gallium Grading Enabling Copper Indium Gallium Selenide Solar Cell with 23.6% Efficiency. *Nat. Energy* **2024**, *9*, 467–478. [CrossRef]
24. Machkih, K.; Oubaki, R.; Makha, M. A Review of CIGS Thin Film Semiconductor Deposition via Sputtering and Thermal Evaporation for Solar Cell Applications. *Coatings* **2024**, *14*, 1088. [CrossRef]
25. Aissani, H.; Helmaoui, A.; Moughli, H. Numerical Modeling of Graded Band-Gap CIGS Solar Celle for High Efficiency. *Int. J. Appl. Eng. Res.* **2017**, *12*, 227–232.
26. Contreras, M.; Tuttle, J.; Du, D.; Qi, Y.; Swartzlander, A.; Tennant, A.; Noufi, R. Graded Band-Gap Cu(In,Ga)Se_2 Thin-Film Solar Cell Absorber with Enhanced Open-Circuit Voltage. *Appl. Phys. Lett.* **1993**, *63*, 1824–1826. [CrossRef]
27. Severino, N.; Bednar, N.; Adamovic, N. Guidelines for Optimization of the Absorber Layer Energy Gap for High Efficiency Cu(In,Ga)Se_2 Solar Cells. *J. Mater. Sci. Chem. Eng.* **2018**, *6*, 147–162. [CrossRef]
28. Huang, C.-H.; Cheng, H.-L.; Chang, W.-E.; Huang, M.Y.; Chien, Y.-J. Investigation of Sputtered Mo Layers on Soda-Lime Glass Substrates for CIGS Solar Cells. *Semicond. Sci. Technol.* **2012**, *27*, 115020. [CrossRef]
29. Dullweber, T.; Anna, G.H.; Rau, U.; Schock, H.W. A New Approach to High-Efficiency Solar Cells by Band Gap Grading in Cu(In,Ga)Se_2 Chalcopyrite Semiconductors. *Sol. Energy Mater. Sol. Cells* **2001**, *67*, 145–150. [CrossRef]
30. Orgassa, K.; Schock, H.W.; Werner, J.H. Alternative Back Contact Materials for Thin Film Cu(In,Ga)Se_2 Solar Cells. *Thin Solid. Film.* **2003**, *431–432*, 387–391. [CrossRef]
31. Lundberg, O.; Bodegård, M.; Malmström, J.; Stolt, L. Influence of the Cu(In,Ga)Se_2 Thickness and Ga Grading on Solar Cell Performance. *Prog. Photovolt.* **2003**, *11*, 77–88. [CrossRef]
32. Ramanathan, K.; Contreras, M.A.; Perkins, C.L.; Asher, S.; Hasoon, F.S.; Keane, J.; Young, D.; Romero, M.; Metzger, W.; Noufi, R.; et al. Properties of 19.2% Efficiency ZnO/CdS/$CuInGaSe_2$ Thin-film Solar Cells. *Prog. Photovolt.* **2003**, *11*, 225–230. [CrossRef]
33. Repins, I.; Contreras, M.A.; Egaas, B.; DeHart, C.; Scharf, J.; Perkins, C.L.; To, B.; Noufi, R. 19.9%-Efficient ZnO/CdS/$CuInGaSe_2$ Solar Cell with 81.2% Fill Factor. *Prog. Photovolt.* **2008**, *16*, 235–239. [CrossRef]
34. Jackson, P.; Hariskos, D.; Lotter, E.; Paetel, S.; Wuerz, R.; Menner, R.; Wischmann, W.; Powalla, M. New World Record Efficiency for Cu(In,Ga)Se_2 Thin-film Solar Cells beyond 20%. *Prog. Photovolt.* **2011**, *19*, 894–897. [CrossRef]
35. Edoff, M.; Schleussner, S.; Wallin, E.; Lundberg, O. Technological and Economical Aspects on the Influence of Reduced Cu(In,Ga)Se_2 Thickness and Ga Grading for Co-Evaporated Cu(In,Ga)Se_2 Modules. *Thin Solid. Film.* **2011**, *519*, 7530–7533. [CrossRef]
36. Lindahl, J.; Zimmermann, U.; Szaniawski, P.; Torndahl, T.; Hultqvist, A.; Salome, P.; Platzer-Bjorkman, C.; Edoff, M. Inline Cu(In,Ga)Se_2 Co-Evaporation for High-Efficiency Solar Cells and Modules. *IEEE J. Photovolt.* **2013**, *3*, 1100–1105. [CrossRef]
37. Witte, W.; Abou-Ras, D.; Albe, K.; Bauer, G.H.; Bertram, F.; Boit, C.; Brüggemann, R.; Christen, J.; Dietrich, J.; Eicke, A.; et al. Gallium Gradients in Cu(In,Ga)Se_2 Thin-Film Solar Cells. *Prog. Photovolt. Res. Appl.* **2015**, *23*, 717–733. [CrossRef]
38. Han, A.; Sun, Y.; Zhang, Y.; Liu, X.; Meng, F.; Liu, Z. Comparative Study of the Role of Ga in CIGS Solar Cells with Different Thickness. *Thin Solid. Film.* **2016**, *598*, 189–194. [CrossRef]

39. Avancini, E.; Carron, R.; Bissig, B.; Reinhard, P.; Menozzi, R.; Sozzi, G.; Di Napoli, S.; Feurer, T.; Nishiwaki, S.; Buecheler, S.; et al. Impact of Compositional Grading and Overall Cu Deficiency on the Near-Infrared Response in Cu(In, Ga)Se_2 Solar Cells. *Prog. Photovolt. Res. Appl.* **2017**, *25*, 233–241. [CrossRef]
40. Essig, S.; Paetel, S.; Friedlmeier, T.M.; Powalla, M. Challenges in the Deposition of (Ag,Cu)(In,Ga)Se_2 Absorber Layers for Thin-Film Solar Cells. *J. Phys. Mater.* **2021**, *4*, 024003. [CrossRef]
41. Li, H.; Qu, F.; Luo, H.; Niu, X.; Chen, J.; Zhang, Y.; Yao, H.; Jia, X.; Gu, H.; Wang, W. Engineering CIGS Grains Qualities to Achieve High Efficiency in Ultrathin Cu(In_x Ga_{1-x})Se_2 Solar Cells with a Single-Gradient Band Gap Profile. *Results Phys.* **2019**, *12*, 704–711. [CrossRef]
42. Gong, J.; Kong, Y.; Li, J.; Wang, K.; Wang, X.; Zhang, Z.; Ding, Z.; Xiao, X. Enhancing Photocurrent of Cu(In,Ga)Se_2 Solar Cells with Actively Controlled Ga Grading in the Absorber Layer. *Nano Energy* **2019**, *62*, 205–211. [CrossRef]
43. Chen, W.-C.; Stolt, L.; Edoff, M. Ga/(Ga + In) Grading Effects on Ultra-Thin (UT) CIGS Solar Cell. In Proceedings of the 2019 IEEE 46th Photovoltaic Specialists Conference (PVSC), Chicago, IL, USA, 16–21 June 2019; Volume 2, pp. 1–3.
44. Nakamura, M.; Yamaguchi, K.; Kimoto, Y.; Yasaki, Y.; Kato, T.; Sugimoto, H. Cd-Free Cu(In,Ga)$(Se,S)_2$ Thin-Film Solar Cell With Record Efficiency of 23.35%. *IEEE J. Photovolt.* **2019**, *9*, 1863–1867. [CrossRef]
45. Solar Frontier | Solar Frontier—Einzigartige CIS-Technologie. Available online: https://www.solar-frontier.eu/en/home/ (accessed on 25 February 2025).
46. MiaSolé—Makers of Lightweight, Flexible, Powerful Solar Cells and Modules. Available online: https://miasole.com/ (accessed on 25 February 2025).
47. Home—Ascent Solar Technologies. Available online: https://ascentsolar.com (accessed on 25 February 2025).
48. Sunflare. Available online: https://www.sunflaresolar.com/ (accessed on 25 February 2025).
49. Eterbright Solar Corp. Available online: https://energypal.com/best-solar-panels-for-homes/eterbright-solar (accessed on 25 February 2025).
50. DS New Energy. Available online: https://www.dsneg.com/ (accessed on 25 February 2025).
51. AVANCIS GmBH. Available online: https://www.avancis.de/en (accessed on 25 February 2025).
52. Scarpulla, M.A.; McCandless, B.; Phillips, A.B.; Yan, Y.; Heben, M.J.; Wolden, C.; Xiong, G.; Metzger, W.K.; Mao, D.; Krasikov, D.; et al. CdTe-Based Thin Film Photovoltaics: Recent Advances, Current Challenges and Future Prospects. *Sol. Energy Mater. Sol. Cells* **2023**, *255*, 112289. [CrossRef]
53. Jäger-Waldau, A. Status of Thin Film Solar Cells in Research, Production and the Market. *Sol. Energy* **2004**, *77*, 667–678. [CrossRef]
54. Jena, I.; Singh, U.P. Advancements in CdTe Thin-Film Solar Cells: Is Doping an Effective Strategy for Performance Enhancement? *Energy Technol.* **2024**, *13*, 2401542. [CrossRef]
55. Lee, T.D.; Ebong, A.U. A Review of Thin Film Solar Cell Technologies and Challenges. *Renew. Sustain. Energy Rev.* **2017**, *70*, 1286–1297. [CrossRef]
56. Zghaibeh, M.; Okonkwo, P.C.; Emori, W.; Ahmed, T.; Mohamed, A.M.A.; Aliyu, M.; Ogunleye, G.J. CdTe Solar Cells Fabrication and Examination Techniques: A Focused Review. *Int. J. Green. Energy* **2023**, *20*, 555–570. [CrossRef]
57. Britt, J.; Ferekides, C. Thin-Film CdS/CdTe Solar Cell with 15.8% Efficiency. *Appl. Phys. Lett.* **1993**, *62*, 2851–2852. [CrossRef]
58. Cunningham, D.; Rubcich, M.; Skinner, D. Cadmium Telluride PV Module Manufacturing at BP Solar. *Prog. Photovolt. Res. Appl.* **2002**, *10*, 159–168. [CrossRef]
59. Bosio, A.; Pasini, S.; Romeo, N. The History of Photovoltaics with Emphasis on CdTe Solar Cells and Modules. *Coatings* **2020**, *10*, 344. [CrossRef]
60. First Solar: A Leading Global Provider of Comprehensive PV Solar Solutions. Available online: https://www.firstsolar.com:443/ (accessed on 25 February 2025).
61. Solar Motion. Available online: http://www.solarmotioning.com/ (accessed on 25 February 2025).
62. CSG PV Tech Co., Ltd. Available online: https://www.csgpvtech.com/en/Default.aspx (accessed on 25 February 2025).
63. Home-Advanced Solar Power (Hangzhou) Inc. Available online: http://www.advsolarpower.com/en/index.php/welcome (accessed on 25 February 2025).
64. CTF Solar GmbH. Available online: https://www.ctf-solar.de/ (accessed on 25 February 2025).
65. Fthenakis, V.; Athias, C.; Blumenthal, A.; Kulur, A.; Magliozzo, J.; Ng, D. Sustainability Evaluation of CdTe PV: An Update. *Renew. Sustain. Energy Rev.* **2020**, *123*, 109776. [CrossRef]
66. Nazir, S.; Ali, A.; Aftab, A.; Muqeet, H.A.; Mirsaeidi, S.; Zhang, J.-M. Techno-Economic and Environmental Perspectives of Solar Cell Technologies: A Comprehensive Review. *Energies* **2023**, *16*, 4959. [CrossRef]
67. Jena, I.; Singh, U.P. Impact of Thin Layer of Copper on Cadmium Telluride and Cadmium Sulfide Thin Films. *J. Mater. Sci Mater. Electron.* **2023**, *34*, 1117. [CrossRef]
68. Tufail, M.; Shah, S.S.A.; Khan, Z.; Ihsan, M.B. Development of 2nd Generation Thin Film Photovoltaics Based on CZTS Absorber Layer and ZnS Window Layer. *Key Eng. Mater.* **2022**, *928*, 177–182. [CrossRef]
69. Delbos, S. Kësterite Thin Films for Photovoltaics: A Review. *EPJ Photovolt.* **2012**, *3*, 35004. [CrossRef]

70. Wang, A.; He, M.; Green, M.A.; Sun, K.; Hao, X. A Critical Review on the Progress of Kesterite Solar Cells: Current Strategies and Insights. *Adv. Energy Mater.* **2023**, *13*, 2203046. [CrossRef]
71. Lee, Y.S.; Gershon, T.; Gunawan, O.; Todorov, T.K.; Gokmen, T.; Virgus, Y.; Guha, S. $Cu_2ZnSnSe_4$ Thin-Film Solar Cells by Thermal Co-evaporation with 11.6% Efficiency and Improved Minority Carrier Diffusion Length. *Adv. Energy Mater.* **2015**, *5*, 1401372. [CrossRef]
72. Sharmin, A.; Kumar, K.; Al Mamun, S.M.M.; Hossain, M. Influence of Annealing Conditions on the Performance of Sputtered Grown CZTS Thin Film Solar Cells. *AIP Adv.* **2022**, *12*, 115025. [CrossRef]
73. Edoff, M. Thin Film Solar Cells: Research in an Industrial Perspective. *AMBIO* **2012**, *41*, 112–118. [CrossRef]
74. Chand, M.M.; Islam, S.; Ahmed, M.T.; Bashar, M.S.; Ahmed, F. Synthesis and Characterization of Lithium-Doped Copper Zinc Tin Sulfide (CZTS) Thin Films. *AIP Adv.* **2023**, *13*, 125225. [CrossRef]
75. Nugroho, H.S.; Refantero, G.; Prima, E.C.; Panatarani, C.; Suyatman; Nugraha, N.; Yuliarto, B. Crystal Structure and Optical Properties of Non-Vacuum Solution-Based Processed Cu_2ZnSnS_4 (CZTS) Thin-Film. *IOP Conf. Ser. Mater. Sci. Eng.* **2021**, *1045*, 012039. [CrossRef]
76. Bhale, D.; Bute, A.; Tokas, R.B.; Phatak, R.; Vishwanadh, B.; Sharma, R.K.; Biswas, A.; Bhattacharyya, D.; Maiti, N. Study of Optical and Structural Properties of CZTS Thin Films Using Copper Capping Layer and Sulfurization to Correct Stoichiometry. *Phys. Scr.* **2024**, *99*, 035903. [CrossRef]
77. Jiang, M.; Wei, F.; Lan, F.; Li, G.; Yan, X. Bandgap Tuning and Morphology Amelioration of Sol-Gel Derived Cu_2ZnSnS_4 (CZTS) Thin Films by Selenium Incorporation. In Proceedings of the 2013 IEEE 39th Photovoltaic Specialists Conference (PVSC), Tampa, FL, USA, 16–21 June 2013; pp. 2602–2604.
78. Rehan, M.; Jeon, H.; Cho, Y.; Cho, A.; Kim, K.; Cho, J.-S.; Yun, J.H.; Ahn, S.; Gwak, J.; Shin, D. Fabrication and Characterization of Cu_2ZnSnS_4 Thin-Film Solar Cells Using a Single-Stage Co-Evaporation Method: Effects of Film Growth Temperatures on Device Performances. *Energies* **2020**, *13*, 1316. [CrossRef]
79. Sun, H.; Huang, J.; Young, T.L.; Cong, J.; Li, J.; Sun, K.; Yan, C.; Soufiani, A.M.; Cui, X.; Nielsen, M.P.; et al. Defect Engineering for Efficient Cu_2ZnSnS_4 Solar Cells via Moisture-Assisted Post-Deposition Annealing. *Adv. Opt. Mater.* **2022**, *10*, 2200607. [CrossRef]
80. Hajara, P.; Rose, T.P.; Jayaraj, M.K.; Saji, K.J. Influence of H_2S on the Growth of Sputter Deposited Cu_2ZnSnS_4 Thin Film. *IOP Conf. Ser. Mater. Sci. Eng.* **2021**, *1166*, 012008. [CrossRef]
81. Guo, Q.; Ford, G.M.; Yang, W.-C.; Walker, B.C.; Stach, E.A.; Hillhouse, H.W.; Agrawal, R. Fabrication of 7.2% Efficient CZTSSe Solar Cells Using CZTS Nanocrystals. *J. Am. Chem. Soc.* **2010**, *132*, 17384–17386. [CrossRef]
82. Todorov, T.K.; Reuter, K.B.; Mitzi, D.B. High-Efficiency Solar Cell with Earth-Abundant Liquid-Processed Absorber. *Adv. Mater.* **2010**, *22*, E156–E159. [CrossRef] [PubMed]
83. Gunawan, O.; Todorov, T.K.; Mitzi, D.B. Loss Mechanisms in Hydrazine-Processed $Cu_2ZnSn(Se,S)_4$ Solar Cells. *Appl. Phys. Lett.* **2010**, *97*, 233506. [CrossRef]
84. Barkhouse, D.A.R.; Gunawan, O.; Gokmen, T.; Todorov, T.K.; Mitzi, D.B. Device Characteristics of a 10.1% Hydrazine-processed $Cu_2ZnSn(Se,S)_4$ Solar Cell. *Prog. Photovolt.* **2012**, *20*, 6–11. [CrossRef]
85. Todorov, T.K.; Tang, J.; Bag, S.; Gunawan, O.; Gokmen, T.; Zhu, Y.; Mitzi, D.B. Beyond 11% Efficiency: Characteristics of State-of-the-Art $Cu_2ZnSn(S,Se)_4$ Solar Cells. *Adv. Energy Mater.* **2013**, *3*, 34–38. [CrossRef]
86. Woo, K.; Kim, Y.; Yang, W.; Kim, K.; Kim, I.; Oh, Y.; Kim, J.Y.; Moon, J. Band-Gap-Graded $Cu_2ZnSn(S_{1-x},Se_x)_4$ Solar Cells Fabricated by an Ethanol-Based, Particulate Precursor Ink Route. *Sci. Rep.* **2013**, *3*, 3069. [CrossRef]
87. Wang, W.; Winkler, M.T.; Gunawan, O.; Gokmen, T.; Todorov, T.K.; Zhu, Y.; Mitzi, D.B. Device Characteristics of CZTSSe Thin-Film Solar Cells with 12.6% Efficiency. *Adv. Energy Mater.* **2014**, *4*, 1301465. [CrossRef]
88. Kim, I.; Kim, K.; Oh, Y.; Woo, K.; Cao, G.; Jeong, S.; Moon, J. Bandgap-Graded $Cu_2Zn(Sn_{1-x}Ge_x)S_4$ Thin-Film Solar Cells Derived from Metal Chalcogenide Complex Ligand Capped Nanocrystals. *Chem. Mater.* **2014**, *26*, 3957–3965. [CrossRef]
89. Olopade, M.; Adewoyin, A.; Olorode, D.; Chendo, M. Effect of Band Gap Grading on the Performance Characteristics of Cu_2ZnSnS_4 Solar Cell. In Proceedings of the 2014 IEEE 40th Photovoltaic Specialist Conference (PVSC), Denver, CO, USA, 8–13 June 2014; pp. 2394–2396.
90. Yang, K.-J.; Son, D.-H.; Sung, S.-J.; Sim, J.-H.; Kim, Y.-I.; Park, S.-N.; Jeon, D.-H.; Kim, J.; Hwang, D.-K.; Jeon, C.-W.; et al. A Band-Gap-Graded CZTSSe Solar Cell with 12.3% Efficiency. *J. Mater. Chem. A* **2016**, *4*, 10151–10158. [CrossRef]
91. Ross, N.; Larsen, J.; Grini, S.; Sarhammar, E.; Vines, L.; Platzer-Björkman, C. $Cu_2ZnSn(S, Se)_4$ Solar Cell Absorbers from Diffusion of Selenium into Annealed Cu_2ZnSnS_4 Absorbers. In Proceedings of the 2016 IEEE 43rd Photovoltaic Specialists Conference (PVSC), Portland, OR, USA, 5–10 June 2016; pp. 492–497.
92. Schnabel, T.; Seboui, M.; Ahlswede, E. Band Gap Tuning of $Cu_2ZnGeS_xSe_{4-x}$ Absorbers for Thin-Film Solar Cells. *Energies* **2017**, *10*, 1813. [CrossRef]
93. Andres, C.; Cabas-Vidani, A.; Tiwari, A.N.; Romanyuk, Y.E. From Sputtered Metal Precursors towards $Cu_2Zn(Sn_{1-x},Ge_x)Se_4$ Thin Film Solar Cells with Shallow Back Grading. *Thin Solid. Film.* **2018**, *665*, 168–172. [CrossRef]

94. Schnabel, T.; Seboui, M.; Ahlswede, E. Evaluation of Different Metal Salt Solutions for the Preparation of Solar Cells with Wide-Gap $Cu_2ZnGeS_xSe_{4-x}$ Absorbers. *RSC Adv.* **2017**, *7*, 26–30. [CrossRef]
95. Wang, K.-C.; Hsu, H.-R.; Chen, H.-S. Study of Surface Sulfurization of $Cu_2ZnSn(S, Se)_4$ Thin Film Solar Cell by Sequential H_2Se-Selenization/H_2S-Sulfurization. *Sol. Energy Mater. Sol. Cells* **2017**, *163*, 31–37. [CrossRef]
96. Schnabel, T.; Seboui, M.; Bauer, A.; Choubrac, L.; Arzel, L.; Harel, S.; Barreau, N.; Ahlswede, E. Evaluation of Different Buffer Materials for Solar Cells with Wide-Gap $Cu_2ZnGeS_xSe_{4-x}$ Absorbers. *RSC Adv.* **2017**, *7*, 40105–40110. [CrossRef]
97. Sahayaraj, S.; Brammertz, G.; Vermang, B.; Schnabel, T.; Ahlswede, E.; Huang, Z.; Ranjbar, S.; Meuris, M.; Vleugels, J.; Poortmans, J. Optoelectronic Properties of Thin Film $Cu_2ZnGeSe_4$ Solar Cells. *Sol. Energy Mater. Sol. Cells* **2017**, *171*, 136–141. [CrossRef]
98. Kaur, K.; Sood, M.; Kumar, N.; Nazari, H.H.; Gudavalli, G.S.; Dhakal, T.P.; Kumar, M. Critical Role of Zn/Sn Ratio to Enhance Cu-Zn-Sn-S Solar Cell Efficiency by Suppressing Detrimental $Cu_{2-x}S$ Secondary Phase. *Sol. Energy Mater. Sol. Cells* **2018**, *179*, 22–30. [CrossRef]
99. Sanchez, T.G.; Regalado-Pérez, E.; Mathew, X.; Sanchez, M.F.; Sanchez, Y.; Saucedo, E.; Mathews, N.R. Ge Doped Cu_2ZnSnS_4: An Investigation on Absorber Recrystallization and Opto-Electronic Properties of Solar Cell. *Sol. Energy Mater. Sol. Cells* **2019**, *198*, 44–52. [CrossRef]
100. Saini, N.; Larsen, J.K.; Sopiha, K.V.; Keller, J.; Ross, N.; Platzer-Björkman, C. Germanium Incorporation in Cu_2ZnSnS_4 and Formation of a Sn–Ge Gradient. *Phys. Status Solidi (A)* **2019**, *216*, 1900492. [CrossRef]
101. Luan, H.; Yao, B.; Li, Y.; Liu, R.; Ding, Z.; Sui, Y.; Zhang, Z.; Zhao, H.; Zhang, L. Influencing Mechanism of Cationic Ratios on Efficiency of $Cu_2ZnSn(S,Se)_4$ Solar Cells Fabricated with DMF-Based Solution Approach. *Sol. Energy Mater. Sol. Cells* **2019**, *195*, 55–62. [CrossRef]
102. Vermang, B.; Brammertz, G.; Meuris, M.; Schnabel, T.; Ahlswede, E.; Choubrac, L.; Harel, S.; Cardinaud, C.; Arzel, L.; Barreau, N.; et al. Wide Band Gap Kesterite Absorbers for Thin Film Solar Cells: Potential and Challenges for Their Deployment in Tandem Devices. *Sustain. Energy Fuels* **2019**, *3*, 2246–2259. [CrossRef]
103. Rondiya, S.R.; Buldu, D.G.; Brammertz, G.; Jadhav, Y.A.; Cross, R.W.; Ghosh, H.N.; Davies, T.E.; Jadkar, S.R.; Dzade, N.Y.; Vermang, B. Revealing the Electronic Structure, Heterojunction Band Offset and Alignment of Cu_2 $ZnGeSe_4$: A Combined Experimental and Computational Study towards Photovoltaic Applications. *Phys. Chem. Chem. Phys.* **2021**, *23*, 9553–9560. [CrossRef]
104. Bermudez, V. Economical and Operational Issues for CIGS in the Future PV Panorama. *Sol. Energy* **2017**, *146*, 85–93. [CrossRef]
105. Meagley, R.; McIntosh, C.; Bob, B.; Ellis, C.; Tinker, L.; Beck, M. *Cadmium Telluride Photovoltaics Perspective Paper*; U.S. Department of Energy—Office of Energy Efficiency & Renewable Energy: Washington, DC, USA, 2025.
106. Li, X.; Ma, B.; Wang, C.; Hu, D.; Lü, Y.; Chen, Y. Recycling and Recovery of Spent Copper—Indium—Gallium—Diselenide (CIGS) Solar Cells: A Review. *Int. J. Min. Met. Mater.* **2023**, *30*, 989–1002. [CrossRef]
107. Giraldo, S.; Jehl, Z.; Placidi, M.; Izquierdo-Roca, V.; Pérez-Rodríguez, A.; Saucedo, E. Progress and Perspectives of Thin Film Kesterite Photovoltaic Technology: A Critical Review. *Adv. Mater.* **2019**, *31*, 1806692. [CrossRef]
108. Khalate, S.A.; Kate, R.S.; Deokate, R.J. A Review on Energy Economics and the Recent Research and Development in Energy and the Cu_2ZnSnS_4 (CZTS) Solar Cells: A Focus towards Efficiency. *Sol. Energy* **2018**, *169*, 616–633. [CrossRef]
109. Stamford, L.; Azapagic, A. Environmental Impacts of Copper-indium-gallium-Selenide (CIGS) Photovoltaics and the Elimination of Cadmium through Atomic Layer Deposition. *Sci. Total Environ.* **2019**, *688*, 1092–1101. [CrossRef] [PubMed]
110. First Solar Inc. *High-Value Recycling Program*; First Solar: Tempe, AZ, USA, 2024; p. 4. Available online: https://www.firstsolar.com/-/media/First-Solar/Sustainability-Documents/Recycling/First-Solar-Recycling-Brochure.ashx?la=en (accessed on 25 February 2025).
111. High-Value Recycling—First Solar. Available online: https://www.firstsolar.com:443/Solutions/Recycling (accessed on 11 March 2025).
112. Badran, G.; Lazarov, V.K. From Waste to Resource: Exploring the Current Challenges and Future Directions of Photovoltic Solar Cell Recycling. *Solar* **2025**, *5*, 4. [CrossRef]
113. Rathore, N.; Panwar, N.L. Strategic Overview of Management of Future Solar Photovoltaic Panel Waste Generation in the Indian Context. *Waste Manag. Res.* **2022**, *40*, 504–518. [CrossRef]
114. Yandem, G.; Willner, J.; Jabłońska-Czapla, M. Integrating Photovoltaic Technologies in Smart Cities: Benefits, Risks and Environmental Impacts with a Focus on Future Prospects in Poland. *Energy Rep.* **2025**, *13*, 2697–2710. [CrossRef]
115. Ravilla, A.; Gullickson, E.; Tomes, A.; Celik, I. Economic and Environmental Sustainability of Copper Indium Gallium Selenide (CIGS) Solar Panels Recycling. *Sci. Total Environ.* **2024**, *951*, 175670. [CrossRef] [PubMed]
116. Zhao, C.; Yu, S.; Tang, W.; Yuan, X.; Zhou, H.; Qi, T.; Zheng, X.; Ning, D.; Ma, M.; Zhu, J.; et al. Advances in CIGS Thin Film Solar Cells with Emphasis on the Alkali Element Post-Deposition Treatment. *Mater. Rep. Energy* **2023**, *3*, 100214. [CrossRef]
117. Liu, W.; Li, H.; Qiao, B.; Zhao, S.; Xu, Z.; Song, D. Highly Efficient CIGS Solar Cells Based on a New CIGS Bandgap Gradient Design Characterized by Numerical Simulation. *Sol. Energy* **2022**, *233*, 337–344. [CrossRef]
118. Nayak, P.K.; Cahen, D. Updated Assessment of Possibilities and Limits for Solar Cells. *Adv. Mater.* **2014**, *26*, 1622–1628. [CrossRef]

119. Han, G.; Zhang, S.; Boix, P.P.; Wong, L.H.; Sun, L.; Lien, S.-Y. Towards High Efficiency Thin Film Solar Cells. *Prog. Mater. Sci.* **2017**, *87*, 246–291. [CrossRef]
120. Boukortt, N.E.I.; Patane, S.; Hadri, B.; Crupi, G. Graded Bandgap Ultrathin CIGS Solar Cells (Invited Paper). *Electronics* **2023**, *12*, 393. [CrossRef]
121. Bär, M.; Bohne, W.; Röhrich, J.; Strub, E.; Lindner, S.; Lux-Steiner, M.C.; Fischer, C.-H.; Niesen, T.P.; Karg, F. Determination of the Band Gap Depth Profile of the Penternary $Cu(In_{(1-x)}Ga_x)(S_ySe_{(1-y)})_2$ Chalcopyrite from Its Composition Gradient. *J. Appl. Phys.* **2004**, *96*, 3857–3860. [CrossRef]
122. Mabvuer, F.T.; Nya, F.T.; Kenfack, G.M.D.; Laref, A. Lowering Cost Approach for CIGS-Based Solar Cell through Optimizing Band Gap Profile and Doping of Stacked Active Layers-SCAPS Modeling. *ACS Omega* **2023**, *8*, 3917–3928. [CrossRef]
123. Gohri, S.; Madan, J.; Pandey, R. Augmenting CIGS Solar Cell Efficiency through Multiple Grading Profile Analysis. *J. Electron. Mater.* **2023**, *52*, 6335–6349. [CrossRef]
124. Dullweber, T.; Hanna, G.; Shams-Kolahi, W.; Schwartzlander, A.; Contreras, M.A.; Noufi, R.; Schock, H.W. Study of the Effect of Gallium Grading in Cu(In,Ga)Se_2. *Thin Solid. Film.* **2000**, *361*, 478–481. [CrossRef]
125. Gorji, N.E.; Perez, M.D.; Reggiani, U.; Sandrolini, L. A New Approach to Valence and Conduction Band Grading in CIGS Thin Film Solar Cells. *Int. J. Eng. Technol.* **2012**, *4*, 573–576. [CrossRef]
126. Lundberg, O.; Edoff, M.; Stolt, L. The Effect of Ga-Grading in CIGS Thin Film Solar Cells. *Thin Solid. Film.* **2005**, *480*, 520–525. [CrossRef]
127. Murata, M.; Hironiwa, D.; Ashida, N.; Chantana, J.; Aoyagi, K.; Kataoka, N.; Minemoto, T. Optimum Bandgap Profile Analysis of Cu(In,Ga)Se_2 Solar Cells with Various Defect Densities by SCAPS. *Jpn. J. Appl. Phys.* **2014**, *53*, 04ER14. [CrossRef]
128. Murata, M.; Chantana, J.; Hironiwa, D.; Aoyagi, K.; Kataoka, N.; Minemoto, T. Theoretical Analysis of Optimum Bandgap Profile of Cu(In,Ga)Se_2 Solar Cells with Optical and Defect Properties. In Proceedings of the Extended Abstracts of the 2013 International Conference on Solid State Devices and Materials, Fukuoka, Japan, 24–26 September 2013; The Japan Society of Applied Physics: Fukuoka, Japan, 2013.
129. Yan, H.; Wang, W.; Luo, J.; Chi, Z.; Gong, J.; Li, J.; Xiao, X. Expanding the Notch Region by Adjusting the Copper Growth Profile for High-Efficiency Flexible Cu(In,Ga)Se_2 Solar Cells. *ACS Appl. Mater. Interfaces* **2024**, *16*, 54171–54177. [CrossRef]
130. Xin, W.; Yuan, M.; Zeng, C.; Lin, R.; Li, D.; Hong, R. Investigation on the Diffusion Mechanism of Ga Element and Regulation of the V-Shaped Bandgap in CIGS Thin Films Based on Magnetron Sputtering with a Quaternary Target. *Solar Energy* **2024**, *273*, 112510. [CrossRef]
131. Wang, J.; Sun, L.; Yuan, Y.; Xing, Y.; Bi, J.; Li, W. A Novel Thermal Annealing Process to Improve Ga Diffusion in CIGS Thin Film Solar Cells. *Appl. Phys. A-Mater. Sci. Process.* **2024**, *130*, 146. [CrossRef]
132. Deo, M.; Chauhan, R.K.; Kumar, M. Optimization and Performance Enhancement of InP/CIGS/CuI Solar Cell Using Bandgap Grading. *J. Opt. India* **2024**, *53*, 1224–1234. [CrossRef]
133. Hameed, T.A.; Cao, W.; Mansour, B.A.; Elzawaway, I.K.; Abdelrazek, E.-M.M.; Elsayed-Ali, H.E. Properties of Cu(In,Ga,Al)Se_2 Thin Films Fabricated by Magnetron Sputtering. *J. Vac. Sci. Technol. A Vac. Surf. Film.* **2015**, *33*, 031201. [CrossRef]
134. Chen, W.; Cao, W.; Hameed, T.A.; Marsillac, S.; Elsayed-Ali, H.E. Properties of Cu(In,Ga,Al)Se_2 Thin Films Fabricated by Pulsed Laser Deposition. *J. Mater. Sci. Mater. Electron.* **2015**, *26*, 1743–1747. [CrossRef]
135. Liu, Y.-D.; Cao, Y.-Q.; Tang, J.-L.; Lin, B. Effects of Alkali Elements on Copper Indium Gallium Aluminum Selenide Flexible Solar Cells Fabricated on Polyimide Substrates. *ACS Appl. Mater. Interfaces* **2024**, *16*, 48629–48638. [CrossRef]
136. Hameed, T.A.; Cao, W.; Abdelrazek, E.M.; El Zawawi, I.K.; Mansour, B.A.; Elsayed-Ali, H.E. Effect of Substrate Temperature on Properties of Cu(In,Ga,Al)Se_2 Films Grown by Magnetron Sputtering. *J. Mater. Sci. Mater. Electron.* **2016**, *27*, 3209–3216. [CrossRef]
137. Nwakanma, O.; Subramaniam, V.; Morales-Acevedo, A. Review on the Effects Due to Alkali Metals on Copper-Indium-Gallium-Selenide Solar Cells. *Mater. Today Energy* **2020**, *20*, 100617. [CrossRef]
138. Malitckaya, M.; Komsa, H.-P.; Havu, V.; Puska, M.J. Effect of Alkali Metal Atom Doping on the $CuInSe_2$ -Based Solar Cell Absorber. *J. Phys. Chem. C* **2017**, *121*, 15516–15528. [CrossRef]
139. Bhatt, V.; Kim, S.-T.; Kumar, M.; Jeong, H.-J.; Kim, J.; Yun, J.-H.; Jang, J.-H. Impact of Na Diffusion on Cu(In,Ga)Se_2 Solar Cells: Unveiling the Role of Active Defects Using Thermal Admittance Spectroscopy. *Thin Solid. Films* **2023**, *767*, 139673.
140. Reinhard, P.; Pianezzi, F.; Bissig, B.; Chirilă, A.; Blösch, P.; Nishiwaki, S.; Buecheler, S.; Tiwari, A.N. Cu(In,Ga)Se_2 Thin-Film Solar Cells and Modules—A Boost in Efficiency Due to Potassium. *IEEE J. Photovolt.* **2015**, *5*, 656–663. [CrossRef]
141. Kim, J.-H.; Kim, M.K.; Gadisa, A.; Stuard, S.J.; Nahid, M.M.; Kwon, S.; Bae, S.; Kim, B.; Park, G.S.; Won, D.H.; et al. Morphological–Electrical Property Relation in Cu(In,Ga)$(S,Se)_2$ Solar Cells: Significance of Crystal Grain Growth and Band Grading by Potassium Treatment. *Small* **2020**, *16*, 2003865. [CrossRef]
142. Chen, Y.-H.; Kuo, R.-T.; Lin, W.-C.; Lai, C.-Y.; Lin, T.-Y. Cesium Modulation in Cu(In,Ga)$(S,Se)_2$ Solar Cells: Comprehensive Analysis on Interface, Surface, and Grain Boundary. *ACS Appl. Mater. Interfaces* **2024**, *16*, 32220–32231.

143. Lin, T.-Y.; Khatri, I.; Matsuura, J.; Shudo, K.; Huang, W.-C.; Sugiyama, M.; Lai, C.-H.; Nakada, T. Alkali-Induced Grain Boundary Reconstruction on Cu(In,Ga)Se_2 Thin Film Solar Cells Using Cesium Fluoride Post Deposition Treatment. *Nano Energy* **2020**, *68*, 104299. [CrossRef]
144. Lin, T.-Y.; Hsieh, C.-F.; Kanai, A.; Yashiro, T.; Zeng, W.-J.; Ma, J.-J.; Hung, S.-F.; Sugiyama, M. Radiation Resistant Chalcopyrite CIGS Solar Cells: Proton Damage Shielding with Cs Treatment and Defect Healing via Heat-Light Soaking. *J. Mater. Chem. A* **2024**, *12*, 7536–7548. [CrossRef]
145. Wands, J.; Bothwell, A.; Tsoulka, P.; Lepetit, T.; Barreau, N.; Rockett, A. Stability of Cu(In_xGa_{1-x})Se_2 Solar Cells Utilizing RbF Postdeposition Treatment under a Sulfur Atmosphere. *Adv. Energy Sustain. Res.* **2023**, *4*, 2300052.
146. Hoang, V.-Q.; Jeon, D.-H.; Kim, S.-Y.; Lee, J.; Son, D.-H.; Yang, K.-J.; Kang, J.-K.; Sung, S.-J.; Hwang, D.-K.; Kim, D.-H. Exploring the Deposition Pathway in the Notch Region of Double-Graded Bandgap ACIGS Solar Cells. *J. Sci.—Adv. Mater. Devices* **2024**, *9*, 100665.
147. Hwang, J.; Park, H.K.; Shin, D.; Jung, I.; Hwang, I.; Eo, Y.-J.; Cho, A.; Park, J.H.; Song, S.; Cho, Y.; et al. Reforming Material Chemistry of CIGS Solar Cells via a Precise Ag Doping Strategy. *J. Mater. Chem. A* **2023**, *11*, 19546–19555.
148. Mori, H.; Chantana, J.; Kawano, Y.; Negami, T.; Minemoto, T. Influence of Silver Introduction into (Ag,Cu)(In,Ga)S_2 Thin Films on Their Physical Properties. *Mater. Sci. Eng. B—Adv. Funct. Solid-State Mater.* **2023**, *297*, 116758.
149. Yao, Y.; Liu, Y.; Ma, J.; Yang, X.; Meng, H.; Liu, F.; Zhang, Y.; Shi, J.; Meng, Q.; Liu, W. Analysis of the Mechanism for Enhanced Crystalline Quality of Wide-Bandgap Cu(In,Ga)Se_2 Films by Pre-Deposited Ag. *J. Mater. Chem. A* **2024**, *12*, 21095–21105.
150. Xu, M.; Yan, S.; Liang, T.; Jia, J.; Yuan, S.; Kou, D.; Zhou, Z.; Zhou, W.; Qi, Y.; Meng, Y.; et al. 16.48% Efficient Solution-Processed CIGS Solar Cells with Crystal Growth and Defects Engineering Enabled by Ag Doping Strategy. *J. Energy Chem.* **2025**, *100*, 59–65. [CrossRef]
151. Keller, J.; Stolt, L.; Donzel-Gargand, O.; Violas, A.F.; Kubart, T.; Edoff, M. Bifacial Wide-Gap (Ag,Cu)(In,Ga)Se_2 Solar Cell with 13.6% Efficiency Using In_2O_3:W as a Back Contact Material. *Solar RRL* **2024**, *8*, 2400430.
152. Gutzler, R.; Kanevce, A.; Wahl, T.; Wessendorf, C.; Hempel, W.; Ahlswede, E.; Hariskos, D.; Paetel, S. Advantage of Zn(O,S) over CdS Buffer for Low-Gap (Ag,Cu)(In,Ga)Se_2 in Tandem Applications. *ACS Appl. Energy Mater.* **2024**, *7*, 3108–3115.
153. Keller, J.; Martin, N.; Donzel-Gargand, O.; Kiselman, K.; Zimmermann, U.; Stolt, L.; Platzer-Bjorkman, C.; Edoff, M. Effect of Ordered Vacancy Compounds on the Carrier Collection in Wide-Gap (Ag,Cu)(In,Ga)Se_2 Solar Cells. *Solar RRL* **2024**, *8*, 2301018.
154. Yoo, H.; Quy, H.V.; Lee, I.; Jo, S.T.; Hong, T.E.; Kim, J.; Yoo, D.-H.; Shin, J.; Commerell, W.; Kim, D.-H.; et al. Understanding of the Relationship between the Properties of Cu(In,Ga)Se_2 Solar Cells and the Structure of Ag Network Electrodes. *Energy Environ. Mater.* **2024**, *7*, e12765.
155. Zouache, R.; Bouchama, I.; Saidani, O.; Ghebouli, M.A.; Akhtar, M.S.; Saeed, M.A.; Boudour, S.; Lamiri, L.; Belgherbi, O.; Messaoudi, M. CGS/CIGS Single and Triple-Junction Thin Film Solar Cell: Optimization of CGS/CIGS Solar Cell at Current Matching Point. *Micro Nanostruct.* **2024**, *189*, 207812.
156. Amin, N.; Sopian, K.; Yahya, M.; Zaharim, A. Significance of Absorber Thickness Reduction in CdTe Thin Film Solar Cells for Promising Terrestrial Usage—From the Perspective of Numerical Analysis. In Proceedings of the 8th WSEAS International Conference on POWER SYSTEMS (PS 2008), Santander, Cantabria, Spain, 23–25 September 2008.
157. Dharmadasa, I.M.; Bingham, P.A.; Echendu, O.K.; Salim, H.I.; Druffel, T.; Dharmadasa, R.; Sumanasekera, G.U.; Dharmasena, R.R.; Dergacheva, M.B.; Mit, K.A.; et al. Fabrication of CdS/CdTe-Based Thin Film Solar Cells Using an Electrochemical Technique. *Coatings* **2014**, *4*, 380–415. [CrossRef]
158. Nagaoka, A.; Swain, S.K.; Munshi, A.H. Review on Group-V Doping in CdTe for Photovoltaic Application. *IEEE J. Photovolt.* **2024**, *14*, 397–413. [CrossRef]
159. Zheng, X.; Kuciauskas, D.; Moseley, J.; Colegrove, E.; Albin, D.S.; Moutinho, H.; Duenow, J.N.; Ablekim, T.; Harvey, S.P.; Ferguson, A.; et al. Recombination and Bandgap Engineering in CdSeTe/CdTe Solar Cells. *APL Mater.* **2019**, *7*, 071112. [CrossRef]
160. Bowman, A.R.; Leaver, J.F.; Frohna, K.; Stranks, S.D.; Tagliabue, G.; Major, J.D. Spatially Resolved Photoluminescence Analysis of the Role of Se in $CdSe_xTe_{1-x}$ Thin Films. *Nat. Commun.* **2024**, *15*, 8729. [CrossRef]
161. Fiducia, T.; Howkins, A.; Abbas, A.; Mendis, B.; Munshi, A.; Barth, K.; Sampath, W.; Walls, J. Selenium Passivates Grain Boundaries in Alloyed CdTe Solar Cells. *Sol. Energy Mater. Sol. Cells* **2022**, *238*, 111595. [CrossRef]
162. Surucu, O.; Surucu, G.; Gasanly, N.M.; Parlak, M.; Isik, M. Exploring Temperature-Dependent Bandgap and Urbach Energies in CdTe Thin Films for Optoelectronic Applications. *Mater. Lett.* **2024**, *373*, 137078. [CrossRef]
163. Tong, C.-J.; McKenna, K.P. Passivating Grain Boundaries in Polycrystalline CdTe. *J. Phys. Chem. C* **2019**, *123*, 23882–23889. [CrossRef]
164. Kranz, L.; Gretener, C.; Perrenoud, J.; Schmitt, R.; Pianezzi, F.; La Mattina, F.; Blösch, P.; Cheah, E.; Chirilă, A.; Fella, C.M.; et al. Doping of Polycrystalline CdTe for High-Efficiency Solar Cells on Flexible Metal Foil. *Nat. Commun.* **2013**, *4*, 2306. [CrossRef]
165. Bloss, W.H.; Pfisterer, F.; Schubert, M.; Walter, T. Thin-film Solar Cells. *Prog. Photovolt.* **1995**, *3*, 3–24. [CrossRef]
166. Kumar, S.G.; Rao, K.S.R.K. Physics and Chemistry of CdTe/CdS Thin Film Heterojunction Photovoltaic Devices: Fundamental and Critical Aspects. *Energy Environ. Sci.* **2013**, *7*, 45–102. [CrossRef]

167. Späth, B.; Lakus-Wollny, K.; Fritsche, J.; Ferekides, C.S.; Klein, A.; Jaegermann, W. Surface Science Studies of Cu Containing Back Contacts for CdTe Solar Cells. *Thin Solid. Film.* **2007**, *515*, 6172–6174. [CrossRef]
168. Chatratin, I.; Dou, B.; Wei, S.-H.; Janotti, A. Doping Limits of Phosphorus, Arsenic, and Antimony in CdTe. *J. Phys. Chem. Lett.* **2023**, *14*, 273–278. [CrossRef]
169. Du, B.; Dobson, K.; McCandless, B.; Nahar, A.; Das, U.; Fields, S.; Arehart, A.; Shafarman, W. Pyrolyzer Assisted Vapor Transport Deposition of Antimony-Doped Cadmium Telluride. In Proceedings of the 2023 IEEE 50th Photovoltaic Specialists Conference (PVSC), San Juan, PR, USA, 11–16 June 2023; pp. 1–5.
170. Wang, A.; Huang, J.; Yan, C.; He, G.; Cui, X.; Yuan, X.; Zhou, S.; He, M.; Qiu, T.; Zhao, C.; et al. Cd-Free High-Bandgap Cu_2ZnSnS_4 Solar Cell with 10.7% Certified Efficiency Enabled by Engineering Sn-Related Defects. *Adv. Funct. Mater.* **2024**, *34*, 2407063. [CrossRef]
171. Nguyen, T.H.; Kawaguchi, T.; Chantana, J.; Minemoto, T.; Harada, T.; Nakanishi, S.; Ikeda, S. Structural and Solar Cell Properties of a Ag-Containing Cu_2ZnSnS_4 Thin Film Derived from Spray Pyrolysis. *ACS Appl. Mater. Interfaces* **2018**, *10*, 5455–5463. [CrossRef] [PubMed]
172. Gour, K.S.; Singh, O.P.; Tawale, J.S.; Singh, V.N. Silver (Ag) Incorporated Cu_2ZnSnS_4 Thin Film for Improved Optical and Morphological Properties. *Superlattices Microstruct.* **2018**, *120*, 54–59. [CrossRef]
173. Saha, U.; Alam, M.K. Boosting the Efficiency of Single Junction Kesterite Solar Cell Using Ag Mixed Cu_2ZnSnS_4 Active Layer. *RSC Adv.* **2018**, *8*, 4905–4913. [CrossRef] [PubMed]
174. Atasoy, Y.; Bacaksız, E.; Çiriş, A.; Olğar, M.A.; Zan, R.; Al-dala Ali, A.M.J.; Küçükömeroğlu, T.; Başol, B.M. Improved CZTSe Solar Cell Efficiency via Silver and Germanium Alloying. *Sol. Energy* **2024**, *267*, 112247. [CrossRef]
175. Honarvar Nazari, H.; Dhakal, T.P. Influence of Ag-Doping on the Performance of Cu_2ZnSnS_4 Solar Cells. *Sol. Energy* **2023**, *253*, 321–331. [CrossRef]
176. Ibrahim, A.; Guchhait, A.; Hadke, S.; Seng, H.L.; Wong, L.H. Silver and Potassium Incorporation in Double-Layer Solution-Processed Cu_2ZnSnS_4 Solar Cell. *ACS Appl. Energy Mater.* **2020**, *3*, 10402–10407. [CrossRef]
177. Naylor, M.C.; Tiwari, D.; Sheppard, A.; Laverock, J.; Campbell, S.; Ford, B.; Xu, X.; Jones, M.D.K.; Qu, Y.; Maiello, P.; et al. Ex Situ Ge-Doping of CZTS Nanocrystals and CZTSSe Solar Absorber Films. *Faraday Discuss.* **2022**, *239*, 70–84. [CrossRef] [PubMed]
178. Li, J.; Shen, H.; Chen, J.; Li, Y.; Yang, J. Growth Mechanism of Ge-Doped CZTSSe Thin Film by Sputtering Method and Solar Cells. *Phys. Chem. Chem. Phys.* **2016**, *18*, 28829–28834. [CrossRef]
179. Atasoy, Y.; Çiriş, A.; Olğar, M.A. Influence of Heating Rate on the Structural and Optical Properties of Silver and Germanium Co-Doped CZTS Thin Film. *Eurasian J. Sci. Eng. Technol.* **2023**, *4*, 10–15. [CrossRef]
180. Oktafiani, A.; Nugroho, F.W.A.; Salsabila, Z.; Sidiq, D.H.; Taufiq, A.; Amrillah, T. The Interplay between Optoelectronic and Magnetic Properties in Co-Doped Cu_2ZnSnS_4 for next-Generation Solar Cell Devices. *J. Phys. D Appl. Phys.* **2024**, *57*, 505303. [CrossRef]
181. Zhang, H.; Ng, Z.-N.; Kang, C.C.; Tan, J.D.; Ariannejad, M.; Bhuiyan, M.A.S.; Chan, K.-Y. Efficiency Enhancement of CZTS Solar Cell with WO_3 Buffer Layer Using CZTSe BSF Layer. *Energy Rep.* **2024**, *12*, 2707–2719. [CrossRef]
182. Riyad, M.N.H.; Sunny, A.; Khatun, M.M.; Rahman, S.; Ahmed, S.R.A. Performance Evaluation of WS_2 as Buffer and Sb_2S_3 as Hole Transport Layer in CZTS Solar Cell by Numerical Simulation. *Eng. Rep.* **2023**, *5*, e12600. [CrossRef]
183. Moustafa, M.; Al Zoubi, T.; Yasin, S. Exploration of CZTS-Based Solar Using the ZrS_2 as a Novel Buffer Layer by SCAPS Simulation. *Opt. Mater.* **2022**, *124*, 112001. [CrossRef]
184. Ghosh, S.; Yasmin, S.; Ferdous, J.; Saha, B.B. Numerical Analysis of a CZTS Solar Cell with MoS_2 as a Buffer Layer and Graphene as a Transparent Conducting Oxide Layer for Enhanced Cell Performance. *Micromachines* **2022**, *13*, 1249. [CrossRef]
185. Chen, Y.; Yuan, Y.; Wu, X.; Wang, Q.; Liu, Y. Novel Buffer Layer on the Performance of CZTS Solar Cells by Numerical Simulation. *Mater. Today Commun.* **2024**, *38*, 108164. [CrossRef]